Mobility and Poisoning of Mass-Selected Platinum Nanoclusters during the Oxygen Reduction Reaction

Jon Ustarroz, Isabel M. Ornelas, Guohui Zhang, David Perry, Minkyung Kang, Cameron L. Bentley, Marc Walker, Patrick R. Unwin**

Department of Chemistry, University of Warwick, Coventry CV4 7AL, U.K.

Nanoscale Physics, Chemistry and Engineering Research Laboratory, University of Birmingham, Birmingham B15 2TT, U.K.

Research Group Electrochemical and Surface Engineering (SURF), Vrije Universiteit Brussel, Pleinlaan 2, 1050 Brussels, Belgium

KEYWORDS

Oxygen Reduction Reaction (ORR); mass-selected nanoclusters; SECCM; carbon corrosion; reactive oxygen species; catalyst poisoning; nanocluster migration;

ABSTRACT

A major challenge in electrocatalysis is to understand the impact of electrochemical processes on the physicochemical properties of nanoparticle or nanocluster (NC) ensembles, especially for complex processes, such as the oxygen reduction reaction (ORR) considered herein. We describe an approach whereby electrocatalysis at a small number of well-defined mass-selected Pt NCs ($Pt_{923\pm37}$, diameter, $d \approx 3$ nm) deposited from a cluster beam source on carbon-coated TEM grids, can be measured by a scanning electrochemical cell microscopy (SECCM) setup, in tandem with a range of complementary microscopy and spectroscopy techniques. The SECCM set up delivers high mass transport rates and allows the effects of transient reactive intermediates to be elucidated for different Pt surface coverage (NC spacing). A major observation is that the ORR activity decreases during successive electrochemical (voltammetric) measurements. This is shown to be due to poisoning of the Pt NCs by carbon/oxygen containing moieties that are produced by the reaction of reactive oxygen intermediates (RIs), generated by ORR, with the carbon support. The effect is most prominent when the Pt surface coverage on the carbon support is low (< 6%). Furthermore, the NC deposition impact energy affects drastically the resulting Pt NC stability during electrochemistry. For lower impact energy, Pt NCs migrate as a consequence of the ORR and are rearranged in characteristic groups on the support. This previously unseen effect is caused by an uneven flux distribution around individual NCs within the ensemble and has important consequences for understanding the stability and activity of NC and nanoparticle arrays.

INTRODUCTION

Understanding electrocatalytic processes in nanoparticle (NP) assemblies is very challenging because of the complex time- and history-dependent structure-activity-mechanism-stability relationships that operate in such systems. This is particularly true for the oxygen reduction reaction (ORR), for which the behavior of the most efficient (Pt and Pt alloy) catalysts is still not completely understood.[1–4] ORR processes on extended Pt surfaces have been extensively studied by employing well-defined Pt single crystals,[2,5,6] but highly dispersed supported NPs that provide large surface areas and enhanced mass-specific activities are needed for practical applications. The effects of catalyst loading and inter-particle interactions on the ORR mechanism, selectivity, stability and the inherent activity remain under discussion and are undergoing revision.[1,4,7–14] A major consideration in the ORR is the balance between the 2 e^- process (leading to H_2O_2) and 4 e^- process (yielding H_2O) and the action of the reactive oxygen intermediates (RIs) produced.

Most experimental studies have been performed on Pt NP dispersions, normally synthesized by wet-chemistry methods, and deposited on high-surface-area carbon materials.[1,15–18] Although there have been important advances in understanding aspects of electrocatalysis,[1,3,15,16,19–21] such approaches incur difficulties, such as relatively poor control over the size, loading and spatial distribution of the catalyst NPs. Moreover, solution-synthesized metal colloids are normally stabilized by ligands and may undergo unwanted aggregation during deposition onto activated carbon, inhibiting catalytic activity.[22] Subtle differences in NP size, loading and geometrical arrangement have recently been shown to affect drastically the catalyst activity[1,7,12] and selectivity (H_2O_2 vs H_2O yield).[8,23,24] Higher ORR activity for higher Pt loading (and hence smaller inter-NP distance) is generally seen, for which there have been two explanations. Most simply, as H_2O_2 is a reaction intermediate of the ORR, a smaller separation between NPs enhances the probability

that H_2O_2 is reduced to H_2O, enhancing the overall activity.[23,24] Another hypothesis is that decreasing the distance between NPs enhances the overlap between the electrical double layers of neighboring NPs, which alters the energetics of adsorbed inhibiting species, which in turn increases the surface-specific activity.[7] Thus, the study of electrochemical processes in *well-defined and characterized* NP geometries has become the priority in the field.[4] To achieve this goal, experiments need to satisfy a number of requirements as outlined below.

First, arrays of Pt NPs with very small size dispersion (ideally, none) and fine control over NP coverage and inter-NP distance are required. This has been achieved by depositing mass-selected clusters by vacuum deposition techniques on a variety of substrates,[7,25] by dendrimer encapsulation,[26] or through the use of arrays of nanoelectrodes as a model.[23,27,28]

Second, the deposited NPs or nanoclusters (NCs) need to be characterized with the highest possible resolution. Although *in-situ* electron microscopy[29,30] and spectroscopy[31] techniques provide an improved understanding of nano-catalyst structure-activity relationships and degradation mechanisms, beam damage[29] or insufficient resolution can impose limitations. *Ex-situ* TEM, especially aberration-corrected HAADF-STEM provides atomic resolution and is a powerful technique to characterize NCs[32,33] even in three dimensions.[33–35] Further, carbon-coated TEM grids (CCTGs) can be used as electrodes for electrochemistry and have been proven suitable for studies of catalyst degradation[21,33,36–50] and electrochemical deposition.[51–54] Notably, Identical Location (IL)-TEM, has been successfully employed to discriminate between different degradation mechanisms such as carbon corrosion, Ostwald ripening, NP migration-aggregation and NP dissolution.[21,36–41,43–46,48–50] However, high resolution TEM studies have not previously been performed on mass-selected NCs after probing their electrocatalytic activity.

Third, for the electrochemical response to be accurately linked with the structure, chemical composition, geometrical arrangement, etc., probing the electrochemistry of a *small number of* NCs is ideal. This has been tackled in different ways. ORR activities have been measured on individual entities, such as single nanowires[55] and NPs[24,56] grown on (ultra)microelectrodes. High resolution electrochemical imaging has been employed to probe other electrocatalytic reactions at individual NPs,[57,58] but these methods are normally limited to NPs of several tens of nm in diameter, and the effects of catalyst loading and inter-particle distance are only just beginning to be addressed.[59] NP impact experiments are a further means of assessing the electrocatalytic activity[60] of individual entities within a small population, but studies relating activity to the structure of a single NP from this type of experiment are rare.[61] The use of nanopipettes to characterise the size of individual NPs and deliver them to a support electrode is a further prospect that will enhance such measurements.[62]

Fourth, it is also relevant to study the ORR under proton-exchange membrane fuel cell (PEMFC)-like conditions, meaning high O_2 mass transport rates, very low catalyst loadings ($\leq$ 1-10 μg/cm^2), and extended potential range (E = 0.5-1 V).[63,64] The study of model catalysts under high mass-transport rates has been achieved by using flow cells,[23,26,65] floating porous gas diffusion electrodes[64] or by growing single sub-micron Pt particles on carbon electrodes.[24]

Here, we present a novel multi-technique approach, designed to address all of the above requirements. Our approach provides electrochemical measurements of a small number of well-defined and characterized NCs, over an extended potential range and under high mass transport rates. The NCs are studied on carbon-coated TEM grids which serve as an electrode and enable subsequent HAADF-STEM imaging of a large proportion of the cluster population subjected to the ORR electrochemical measurements, as well as unperturbed clusters, revealing new

information of the effect of electrochemistry on the arrangement of NPs on surfaces. These studies are further complemented with XPS measurements. Together with the electrochemical measurements, these studies reveal many insights on catalyst and support degradation processes.

RESULTS AND DISCUSSION

Depositing mass-selected clusters from a cluster beam source provides control over NC size and density independently.[66,67] Furthermore, the binding strength between NCs and the substrate can be tuned by the voltage that is applied to the substrate during deposition.[68] In this work, mass-selected Pt NCs of 923 ± 37 atoms (Pt_{923}; $d \approx 3$ nm) were synthesized in a magnetron-sputtering,[67] gas-aggregation cluster beam source and deposited on CCTGs with two different impact energies (0.54 and 1.6 eV/atom) and two different deposition coverages. More details are given in the Methods section and Supporting Information, Section S1. Further information can be found elsewhere.[66,67] Representative HAADF-STEM images, size distributions, and NC distribution parameters (diameter, *d,* particle density, *N* and surface coverage, *SC*) are shown in the Supporting Information, Section S2. For clarity, hereafter, we refer to these samples as Low Density - Low Impact Energy (LD-LIE, $N \approx 5.2 - 6.1 \times 10^{11}$ cm^{-2}, $SC \approx 5.5 \pm 1.1\%$), Low Density - High Impact Energy (LD-HIE, $N \approx 6.3 - 6.5 \times 10^{11}$ cm^{-2}, $SC \approx 6.1 \pm 1.0\%$), and High Density – High Impact Energy (HD-HIE, $N \approx 2 - 2.3 \times 10^{12}$ cm^{-2}, $SC \approx 36.9 \pm 1.9\%$). These distributions correspond to Pt loadings of, approximately, 0.1 μg/cm^2 and 0.85 μg/cm^2 for the low and high density, respectively, which are in the range or even lower than the catalyst loadings presently been investigated for PEMFCs (≤ 1-40 μg/cm^2).[1,64]

The Pt/CCTGs were studied with a scanning electrochemical cell microscopy (SECCM) setup (Figure 1a), using a dual-channel pipette of approximately 1 μm in diameter,[69–71] with each barrel

of the probe containing a Pd-H_2 quasi-reference counter electrode (QRCE), filled with 0.1 M $HClO_4$ supporting electrolyte. The CCTG was placed on an inverted optical microscope, allowing micron spatial resolution optical visualization of the positions where the electrochemical measurements were performed (Figure 1b); see Methods section for further information. The working electrode probe was brought into meniscus contact with the CCTG to create a working electrode of ca. 1 μm diameter. By means of this approach, the electrochemical activity of approximately 5000 to 16000 clusters (depending on the cluster density) was measured. *Ex-situ* HAADF-STEM analysis could subsequently be performed in the area exposed to the electrochemical process, as such areas appeared brighter (Figure 1c) as a consequence of the ORR measurements (this phenomenon is discussed later). This approach also allowed the study of catalyst NC degradation processes, since a representative region 'just outside' the area probed electrochemically (equivalent to the situation before electrochemistry) could also be imaged for comparison.

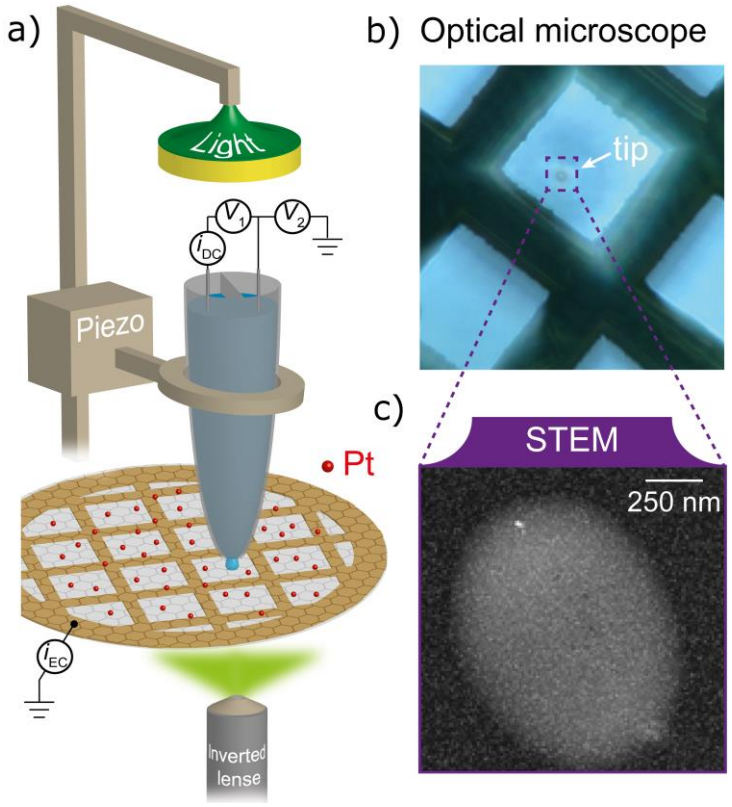

Figure 1 a) Schematic of the carbon-coated TEM grid (with Pt NCs) mounted on an inverted optical microscope equipped with a dual-barrel SECCM setup. b) Optical microscope image showing the exact position where the SECCM tip is landed on the TEM grid. c) HAADF-STEM image showing the footprint of the area that was in contact with the SECCM meniscus (≈ 1 μm^2)

The diffusion of O_2 to the CCTG surface is both through the electrolyte solution (from the pipette) and across the aqueous-air phase[72] (see also scheme in Figure 2a), providing mass-transport rates of the order of 0.1 cm s^{-1} or higher,[72] at least an order of magnitude higher than with the standard rotation rates employed in an RDE setup (1000 - 2000 rpm).[19] This 3 phase arrangement mimics that found in PEMFCs.

Oxygen reduction reaction on mass-selected Pt NCs

Figures 2b and 2c show cyclic voltammograms (CVs) recorded at 10 mV s^{-1} in air-saturated 0.1 M $HClO_4$ solution for the two different particle densities and impact energies during deposition. The currents were normalized: (a) by the footprint of the droplet (see Figure 1, bottom right), in order to obtain the geometrical current densities; and (b) by the Pt surface area of each individual experiment, as obtained from STEM imaging (see, for example Figure S2, Supporting Information, Section S2) considering each nanocluster as hemispherical.[7]

Although electrochemical cleaning is normally carried out to remove contamination from the Pt NCs, accelerating the ORR kinetics, it can also affect the structure and organisation of the NCs on the surface. To demonstrate this, a standard electrochemical cleaning procedure was carried out on LD-HIE and HD-HIE samples and was shown to reduce the overpotential for the ORR onset in approximately 80 mV, but to cause significant changes in the Pt NC distribution (see Supporting Information, Section S3). Therefore, we did not apply any cleaning treatment to the substrates after NC deposition, to avoid any possible change in the structure and organisation of the NCs on the surface.

Figures 2b and 2c show that, in the absence of electrochemical cleaning, the onset potential of the ORR is about 0.7 V for the high density sample and shifts to about 0.6 V for the two low density samples. Similar onset potentials have been reported for the ORR on extended Pt surfaces (flame annealed and protected by a droplet of water before study, and also subjected to *in-situ* electrochemical cleaning) under high mass transport conditions[72] and on small Pt nanoclusters (d < 1 nm).[8,25,65] More specifically, an onset of approx. 0.7 V vs RHE can be found for a distribution of clusters of d ≈ 1 - 2 nm in a RDE configuration (900 rpm) with a Pt loading of 2.5 μg_{Pt} cm^{-2},[8]

between 3 and 25 times higher than the loadings reported in the current manuscript (0.1 and 0.85 μg_{Pt} cm^{-2}). The ORR proceeds in kinetic or mixed control over an extended potential range, down to E ≈ 0.2 V. This behavior has been reported when the ORR is measured under high mass transport rates.[23,24,26,72] At E ≈ 0.2 V, the current starts to level-off. At E ≈ 0.05 V, before having reached a plateau, the current magnitude increases drastically, which can be attributed to H_2 evolution.

For the SECCM configuration with a tip of this size, a limiting current of roughly 6 mA/cm^2 would be expected[72] for a 4 e^- ORR process on the HD-HIE sample where essentially complete diffusional overlap would occur (Pt surface coverage ca. 37%). However, the apparent limiting current measured for the HD-HIE sample is only about 2.7 mA/cm^2. It is known that hydrogen adsorbs in Pt at E ≤ 0.3 V and that, in this potential range, the 4e^- ORR is no longer possible due to adsorbed hydrogen.[6,15,73–77] In this potential range, a 2e^- process would be expected, in line with the currents measured. For the LD samples, the maximum current densities measured before H_2 evolution proceeds are, approximately, 0.3 mA/cm^2. Such low current densities cannot be related to O_2 diffusion limitation, even if a 1e^- reduction was considered. With low Pt NC coverage (< 6%) and the high mass transport rates provided by the SECCM setup, the current limitation arises from the blocking of active sites by adsorbed hydrogen and a poisoning of the Pt surface, even during the course of the first voltammetric scan (discussed later). This would also explain why the current plateau is less evident for the LD samples than for the HD-HIE sample.

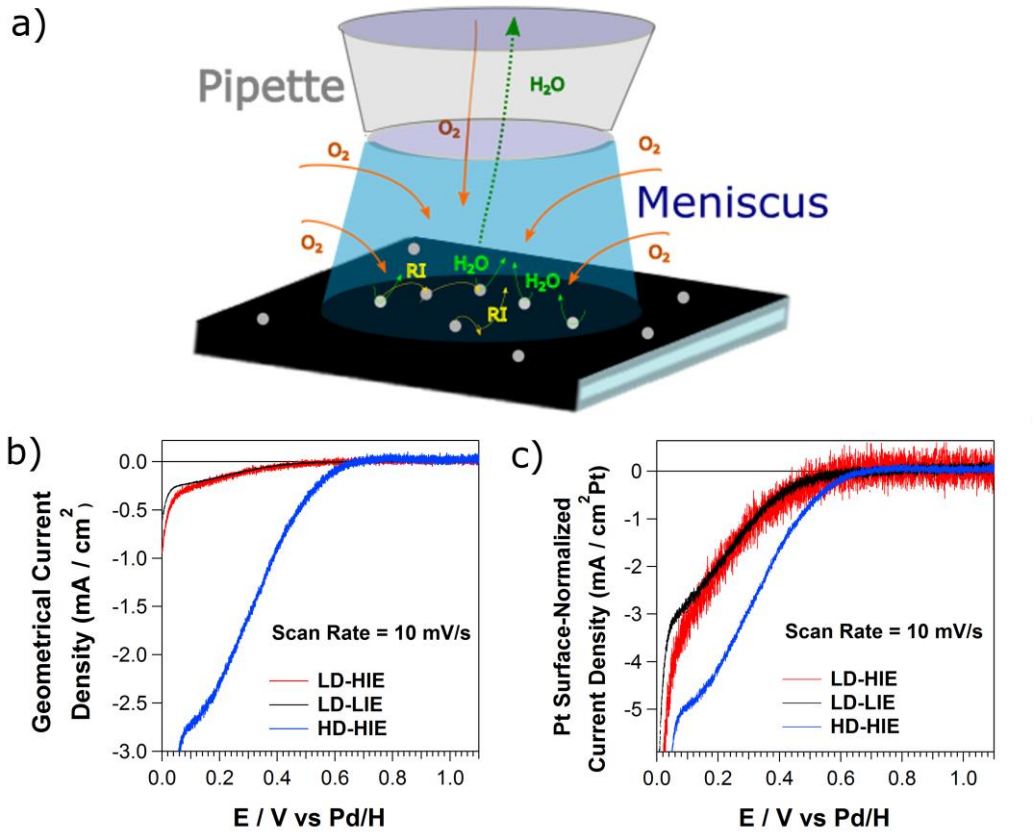

Figure 2 a) Schematic of the fluxes of reactants and products in the SECCM setup. The flux of O_2 towards the electrode is provided by diffusion down the barrels of the pipette as well as across the air-water interface. The flux of RIs and H_2O out from the interface is only possible up the barrel. RI: reaction intermediate. Linear sweep voltammograms (LSVs) recorded with a dual-barrel SECCM setup on a carbon-coated TEM grid with mass-selected Pt NCs, deposited with various NC densities and impact energies: geometrical (b) and Pt surface normalized (c) current densities. All the voltammograms were recorded at 10 mV s^{-1} in an air-saturated 0.1 M $HClO_4$ solution.

When normalized by the Pt surface area (Figure 2c), the CVs also show that a slightly lower current density for the samples with lower Pt NP coverage, over the whole potential range. This further emphasizes that, under these conditions (low Pt NP coverage (< 6%) and high mass transport rates), there is a higher probability that RIs leave the catalyst/solution interface without

being further reduced,[8,23,24,26] resulting in a lower average number of electrons transferred than in the HD-HIE sample, as well as promoting side reactions with the carbon support. The mass transport asymmetry of the experimental setup (enhanced flux of reactants due to gas/liquid transfer, see Figure 2a), whereas reaction intermediates (RIs) and products are confined to the solution, promotes this effect, as discussed later.

In addition, it must be noted that the Pt surface-normalized current densities for the two different LD samples are very similar, independent of the deposition impact energy. This means that subtle differences in the shape (i.e., aspect ratio) of the clusters caused by the different impact energies (see Supporting Information, Section S2) do not influence significantly the ORR activity. Further, Figures 3a and 3b show consecutive scans recorded at 10 mV s^{-1} on the LD-LIE (3a) and LD-HIE (3b) samples. In both cases, a decrease of the electrochemical current across the entire potential range, is evident after each scan, *regardless of the cluster impact energy*.

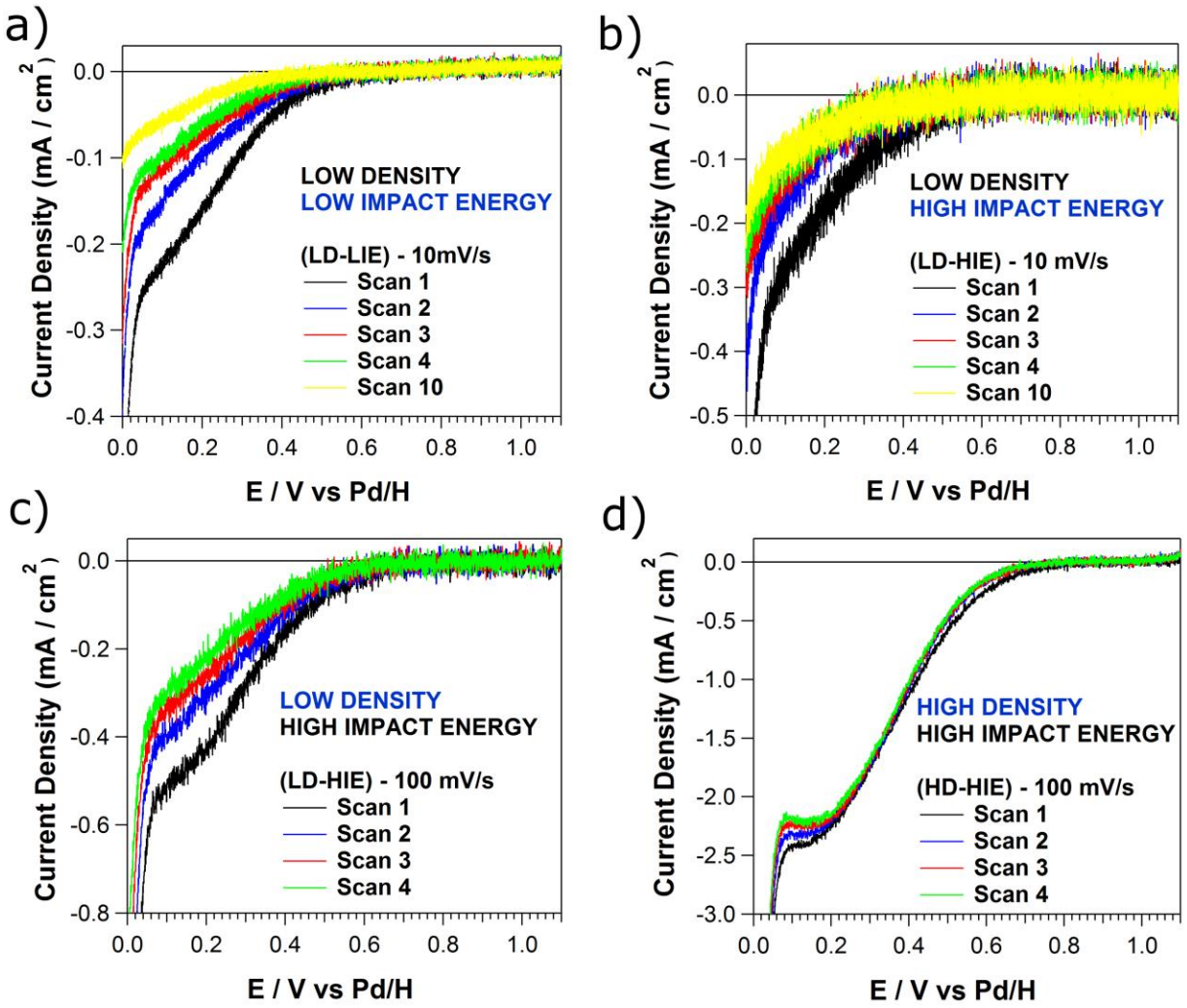

Figure 3 Consecutive LSVs recorded on a carbon-coated TEM grid with mass-selected Pt NCs, deposited with (a) low NC density and low impact energy, (b and c) low NC density and high impact energy and (d) high density and high impact energy. The voltammograms were recorded at (a,b) 10 mV s^{-1} and (c,d) 100 mV s^{-1} in an air-saturated 0.1 M $HClO_4$ solution.

Figures 3c and 3d show consecutive scans recorded at 100 mV s^{-1} on the LD-HIE (3c) and HD-HIE (3d) samples. A comparison of Figures 3c and 3b reveals that the current densities measured at 100 mV s^{-1} (3c) are higher than these at 10 mV s^{-1} (3b), and the decrease in activity with each

voltammetric scan is more gradual. This reinforces the idea that, when the scan rate is low (long timescale), the Pt surface is more susceptible to poisoning. In contrast, there is almost no change in current-voltage response for the HD-HIE sample at 100 mV s^{-1} (3d). We can therefore conclude that *a decrease of the ORR activity after consecutive CV scans, and even during the first scan for low scan rates, occurs for very low Pt surface coverage.* In the next sections we examine the possible causes of the electrochemically induced activity loss.

Decrease of the ORR activity under high mass-transport conditions

The decrease of the electrochemical activity of carbon supported Pt NP or NC catalysts, Pt/C, during ORR has been reported extensively.[3,21,37,39,44,78] The degradation mechanisms considered are Pt dissolution, Pt cluster migration-aggregation, Ostwald Ripening, Pt surface poisoning and carbon corrosion which could induce weakening of the Pt-C surface interaction, inducing NP migration or the detachment of Pt NPs. In principle, the decrease of current density with consecutive scans reported in Figure 3 could be caused by any of these mechanisms.

Pt NCs (d < 1nm) are particularly prone to surface passivation by organic adsorbates,[25] among which CO is the most extensively studied.[78] Carbon is oxidized to CO_2 electrochemically[79] at E > 0.207 vs RHE and although the kinetics are very slow at E ≤ 1V,[80] this process is catalyzed by small Pt NCs.[81] The carbon support may also be oxidized chemically by the attack of RIs,[82–86] which can be generated transiently in the ORR.

The most prominent RI generated through the ORR is hydrogen peroxide, which may attack carbon chemically.[82,84,85] To assess whether this was important for the processes studied herein, a series of cyclic voltammograms were run with different amounts of H_2O_2 on the LD-HIE working electrode sample (Section S4, Figure S7 of the Supporting Information) to discern whether H_2O_2

was involved in the poisoning of the Pt NCs. H_2O_2 did not affect the ORR current-voltage response or the pattern of voltammetric deterioration with scan number. Thus, any catalyst poisoning is as a consequence of the ORR and is related to RI by-products other than H_2O_2.

The superoxide anion radical (O2•-)[87–90] hydroxyl radical (•OH),[91–93] and hydroperoxyl radical (•OOH)[94] have all been detected as products from the ORR in PEMFCs[91,95,96] or in aqueous alkaline or neutral solutions.[89,90,94,97–99] They have also been detected directly[88,94] or indirectly[99] in small concentrations and suggested[75,76,100] as ORR reaction intermediates in acidic solutions. Whereas at an extended Pt electrode, these RIs will be further reduced to hydrogen peroxide or water at vicinal Pt sites, due to the high mass transport rates in an SECCM setup and the small size and low coverage of the Pt NCs, these RIs can readily diffuse to, and react with, the carbon support near the NCs,[81] and the product(s) of this reaction (including CO) may adsorb on, and poison, the Pt NCs.[84] This effect would obviously be more prominent for the LD NC ensembles, as found herein.

XPS measurements were performed on the LD-HIE and HD-HIE samples before and after a series of CVs (200 scans at 200 mV s^{-1}) to investigate the effect of the ORR on the chemical composition of the carbon support.[36,80,101] The relative composition of Pt, C and O before and after ORR is summarized in the Supporting Information, Section S5, Table S3. Interestingly, the oxygen to carbon ratio increased significantly after the ORR for the LD-HIE case (from 0.16 to 0.38) whereas it stayed almost constant in the HD-HIE case (change from 0.25 to 0.28). Figure 4 shows XPS spectra between the binding energies E_b = 278 eV and E_b = 296 eV, corresponding to the C 1s peak and its deconvolution into different chemical bonds. It can be seen by inspection of Figures 4a (before ORR) and 4b (after ORR) that the chemical signature of carbon changes significantly for the LD-HIE sample. As detailed in Supporting Information, Section S5, Table S4, the relative

amount of graphitic carbon decreased significantly (from 53% to 22%), whereas the contribution from C-C/C-H and C-O increased significantly (from 34% to 53% and from 6% to 14%, respectively). The contribution of O=C-OH and C=O remained almost unchanged, before and after electrochemistry (4-7% and 3% respectively). In contrast, for the HD-HIE sample (Figures 4c and 4d), the ratio between graphitic carbon and C-C/C-H, was largely unaffected by the ORR (the contribution of graphitic carbon slightly decreases from 48% to 40% and the contribution of C-C/C-H remains about 33%). An increase in C-O is apparent (from 12% to 17%) and the relative contribution of O=C-OH and C=O remains almost unchanged (3-5% in both cases).

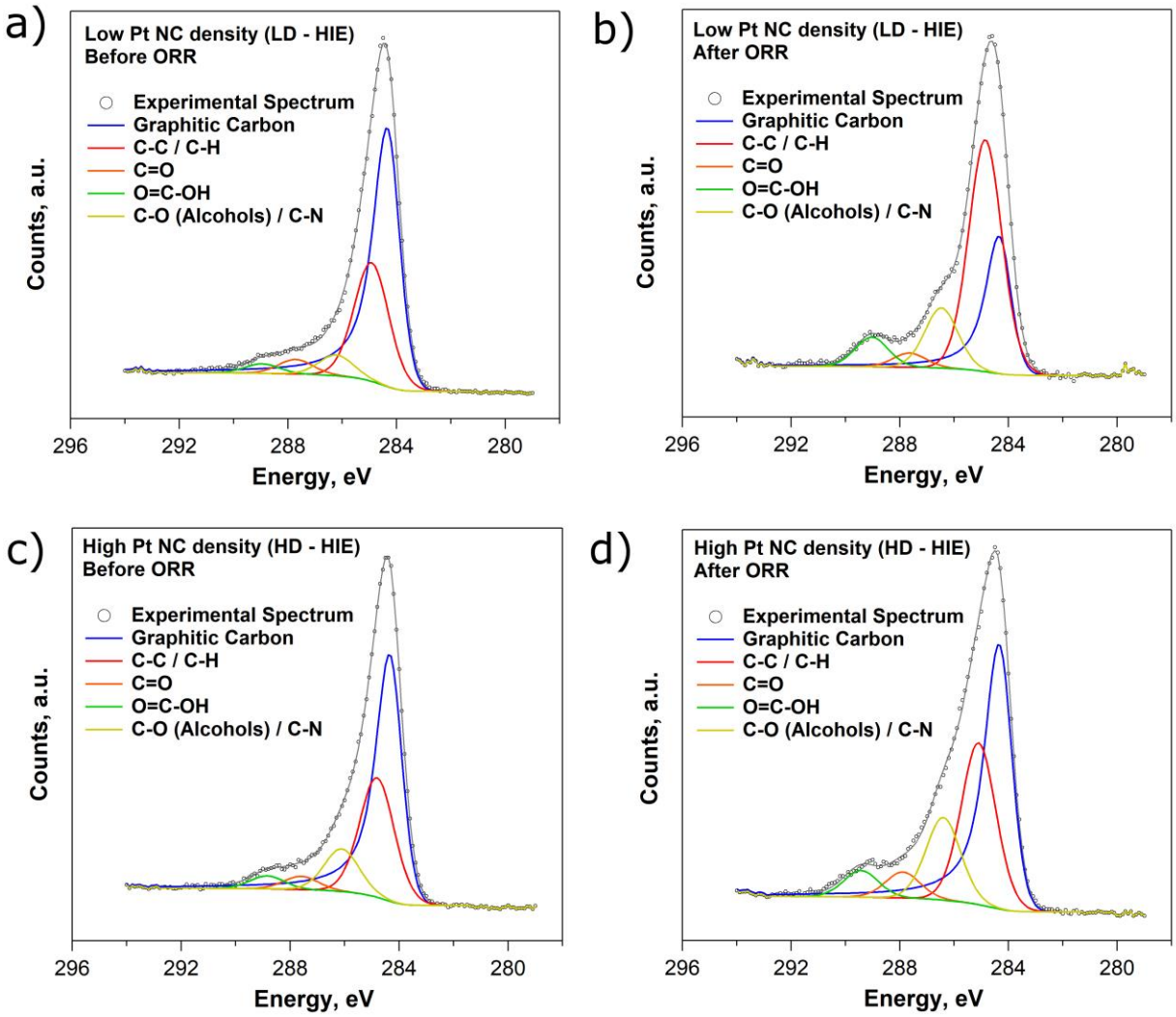

Figure 4 XPS spectra of the C 1s peak from a carbon-coated TEM grid with mass-selected Pt NCs deposited with (a,b) low NC density and (c,d) high NC density, (a,c) before and (b,d) after 200 voltammetric scans from $E = 0$ V to $E = 1.1$ V vs Pd-H_2 at 200 mV s^{-1}.

The different evolution of the surface chemistry of the carbon support for the LD and HD samples, after driving the ORR for the same time and extent, is clear evidence of differences in the ORR process and proportions of by-products (RIs) that depend solely on the density and

geometrical arrangement of NCs on the carbon support. When the coverage of Pt NCs is low, RIs are more likely to escape from the Pt surface and chemically attack the carbon support. The hydroxyl (•OH) or hydroperoxil (•OOH) radical have been suggested as the cause of increase in oxygen containing functional groups of carbon supports after ORR in acidic solutions,[36] and the •OH radical preferentially attacks sp^2 graphitic carbon.[83] When the coverage of Pt NCs is higher (HD-HIE), RIs are less likely to attack the carbon support, because this process is in parallel with the further reduction of RIs species at the higher coverage of neighboring Pt NCs. Note that XPS spectra of the same CCTGs with no Pt NCs were also acquired before and after the same CV cycle regime (not shown) and no changes in the carbon C 1s peak were detected. Therefore, it is clear that the RIs that attack the carbon support are formed at the Pt NCs during the ORR and that the extent of attack increases as the Pt NC coverage decreases.

Figure 5 shows XPS spectra between the binding energies E_b = 63 eV and E_b = 82 eV, corresponding to the Pt 4f peak and its deconvolution into metallic and oxidized Pt for both the LD-HIE sample, before (a) and after (b) the ORR, and the HD-HIE sample, before (c) and after (d) ORR. The relative contributions of both oxidation states are shown in the Supporting Information, Section S5, Table S5. Only metallic Pt is seen before the ORR, for both samples. Since, the CVs are finished at E = 1 V, it would be expected that, after the ORR cycles, the Pt NCs would be partially oxidized. However, although an error of ±2% must be borne in mind, it is evident from Figure 5 and Table S5 of the Supporting Information that the ratio of oxidized to metallic Pt is larger in the LD (0.15 ± 0.03) than in the HD (0.03 ± 0.02) case. We note that the HD sample consists of both isolated and aggregated clusters, but a detailed analysis of the STEM images indicates that the Pt surface to volume ratio of the LD sample is only 1.25 times higher than the HD sample, which does not account for the large differences in oxidized to metallic Pt

ratios between these two samples. Rather, these data suggest that carbon surface oxides, from the carbon corrosion process, are bound to the Pt NCs and explain the severe poisoning seen, for the LD samples.

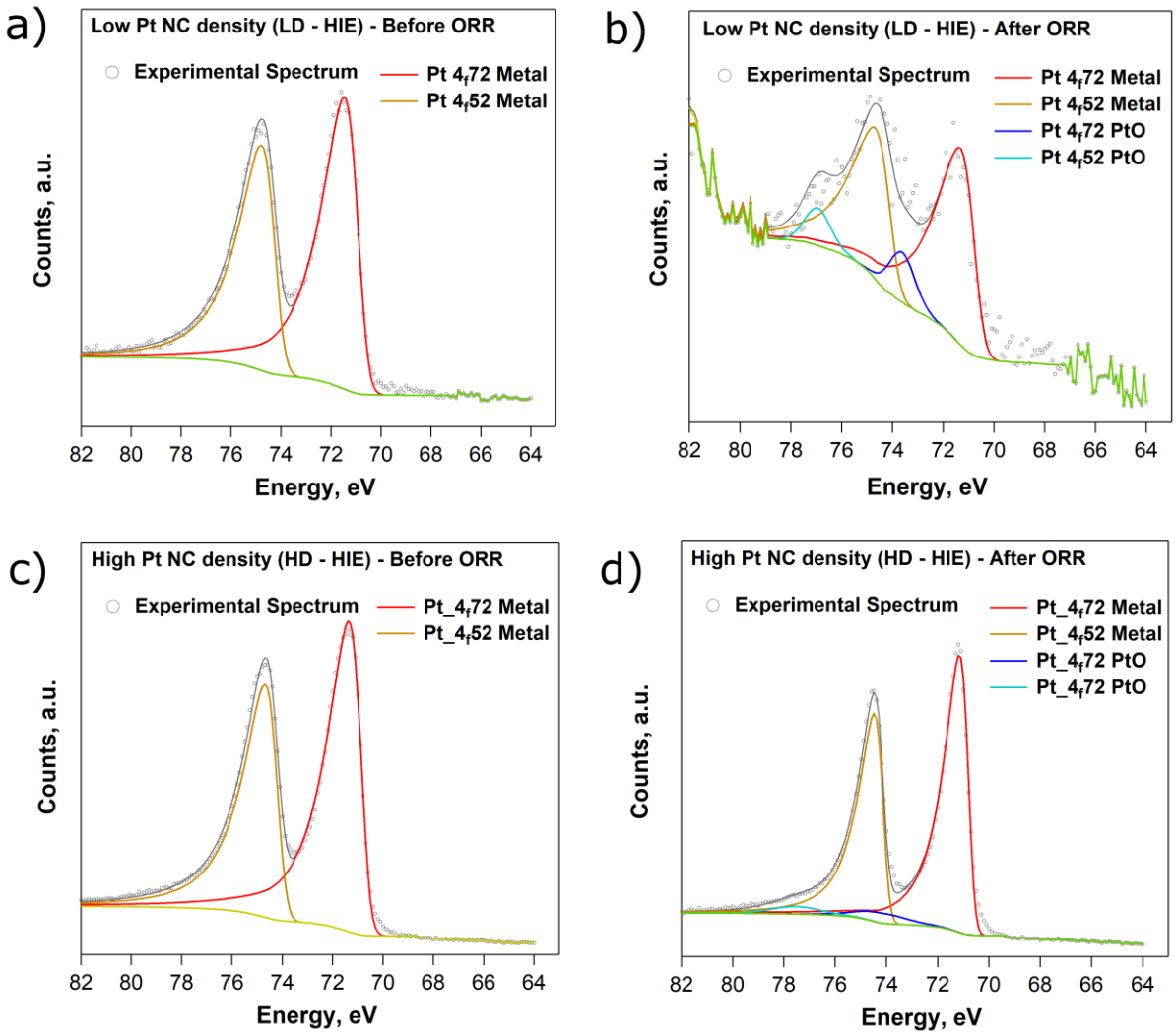

Figure 5 Figure 4 XPS spectra of the Pt 4f peak recorded on a carbon-coated TEM grid with mass-selected Pt NCs deposited with (a,b) low NC density and (c,d) high NC density, (a,c) before and (b,d) after 200 scans from $E = 0$ V to $E = 1.1$ V vs Pd-H_2 at 200 mV s^{-1}.

Further analysis of the Pt 4f peak revealed a difference in the binding energy of the oxidized Pt contribution between the HD (E_b = 74.2 eV) and LD (E_b = 73.6 eV) samples, with a larger peak separation for the HD case. The low amount of Pt in the LD case and the consequent noise of the Pt 4f XPS spectra, does not allow us to draw definitive conclusions about the Pt surface state, but it is clear that, when the Pt NC density is low, driving the ORR leads not only to a higher amount of oxidized Pt, but also a surface that is chemically distinct from the HD case.

HAADF-STEM analysis

A deterioration of the carbon support, as identified in the previous section, has been related to the detachment or migration-aggregation of Pt NCs,[36] which induce electrochemical activity losses. To reveal whether Pt NC migration-aggregation, detachment, dissolution or Ostwald Ripening contribute to the gradual loss of activity seen in the voltammetric scans (Figure 3), a thorough microscopic analysis of the Pt NC distributions was performed just outside (equivalent to "before ORR") and inside (equivalent to "after ORR") the areas where the ORR was executed for different times (voltammetric scan rates). This analysis considered the effect of deposition impact energy on NC stability.

Figure 6 shows representative HAADF-STEM images and corresponding size and cumulative Nearest Neighbor Distance (NND) histograms of the LD-HIE sample after a series of cyclic voltammograms. Figure 6a displays HAADF-STEM images taken just outside two SECCM regions where 50 scans at 500 mV s^{-1} (first row) and 15 scans at 10 mV s^{-1} (second row) were performed, while Figure 6b shows characteristic images taken inside these spots. At first sight, there are no obvious differences in NC size or geometrical arrangement between these neighboring areas.

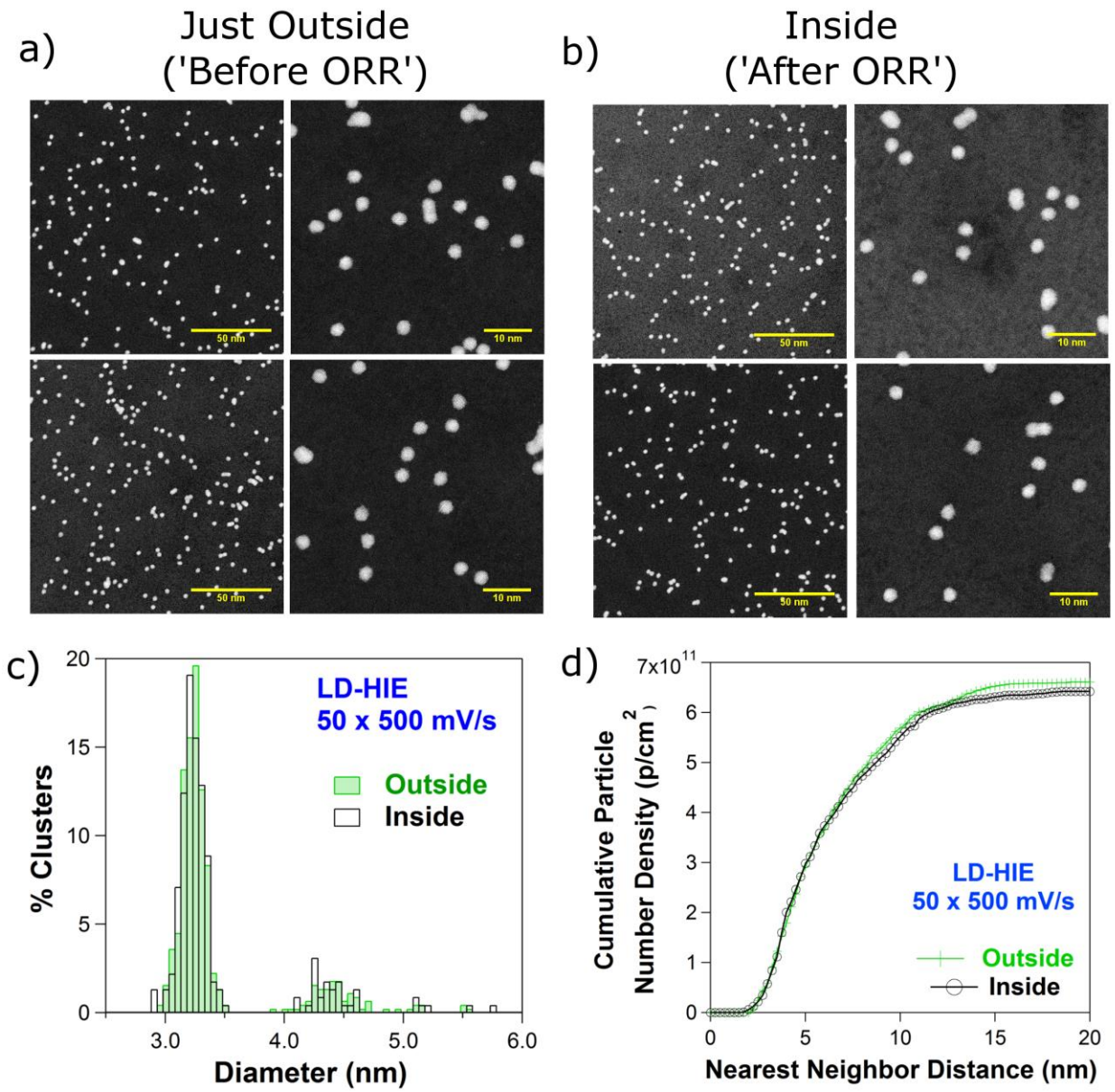

Figure 6 Representative HAADF-STEM images of Pt NCs deposited on a carbon coated TEM grid with low NC density and high impact energy (a) before and (b) after (first row) 50 scans at 500 mV s^{-1} and (second row) 15 scans at 10 mV s^{-1}. Pt NC (c) size and (d) cumulative nearest neighbor distance histograms before and after 50 scans at 500 mV s^{-1}.

Figures 6c and 6d show the particle size and cumulative NND histograms for the case of 50 scans at 500 mV s^{-1}. The particle size is almost identical outside ('before ORR') and inside (after 'ORR') the electrochemically measured area. The geometrical NC arrangement, as indicated by the cumulative NND histogram, is also unchanged by the electrochemistry. This was found for the whole range of cyclic voltammograms recorded for different number of cycles and scanning rates of the LD-HIE sample (see Supporting Information, Section S6).

The data in Figure 6 are highly significant: one can rule out Ostwald Ripening, Pt dissolution and Pt NC detachment as being responsible for the loss of electrochemical activity. NC migration-aggregation can also be excluded, since there is no increase in the number of aggregates (Supporting Information, Section S7, Figure S11a). A similar analysis was performed on the HD-HIE sample. There were no obvious changes in the size distribution or geometrical arrangement (including sintering) of the Pt NCs (Supporting Information Section S7).

Figure 7 shows representative HAADF-STEM images of the LD-LIE sample after cycling through the ORR with different scan rates. Figure 7a displays HAADF-STEM images from the region immediately outside two SECCM spots where 20 voltammetric scans at 50 mV s^{-1} (first row) and 50 scans at 100 mV s^{-1} (second row) were carried out. Figure 7b shows characteristic HAADF-STEM images inside the spots. Substantial differences in the geometrical arrangement of NCs after voltammetric scanning are found: the NCs become arranged in groups of several NCs (Figure 7b), with sometimes 15 or more NCs per group.

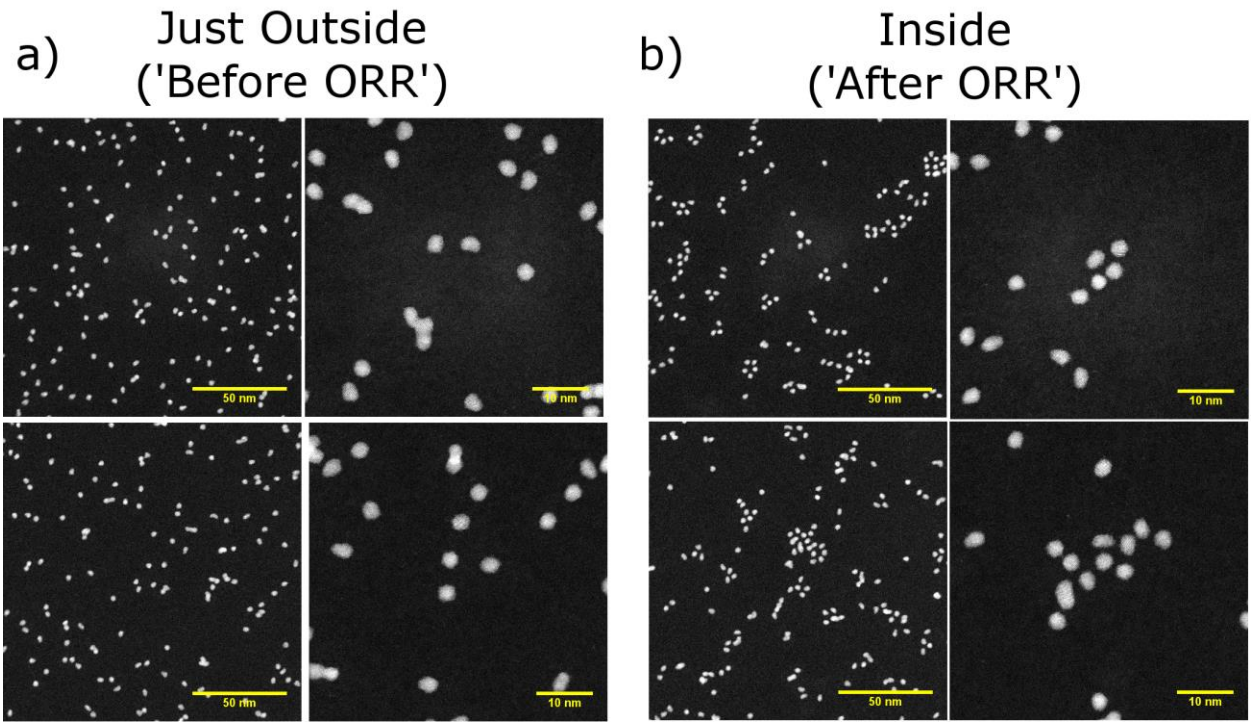

Figure 7 Representative HAADF-STEM images of Pt NCs deposited on a carbon coated TEM grid with low NC density and low impact energy (a) before and (b) after (first row) 20 scans at 50 mV s^{-1} and (second row) 50 scans at 10 mV s^{-1}.

The drastic changes in the Pt NC arrangement for the LD-LIE sample, upon electrochemical cycling, are quantitatively represented by the NND histograms shown in Figures 8a and 8b and the cumulative NND histograms shown in the Supporting Information, Section S8, figure S12b and S12c. Whereas before cycling, the NND is broadly distributed between 3 and 15 nm, after driving the ORR, approximately 75% of the clusters are separated by less than 5.5 nm from their nearest neighbor.

To quantitatively assess the arrangement of the Pt NCs, an analysis of the Nth Nearest Neighbor Distance (with N from 1 to 15) before and after 50 voltammetric scans at 100 mV s^{-1} is shown in Figure 8c. It is clear that the interparticle distribution after cycling through the ORR shifts to lower

values, being particularly evident for the 5 nearest neighbors, but also seen for higher neighbor numbers, such as 10th and 15th neighbors.

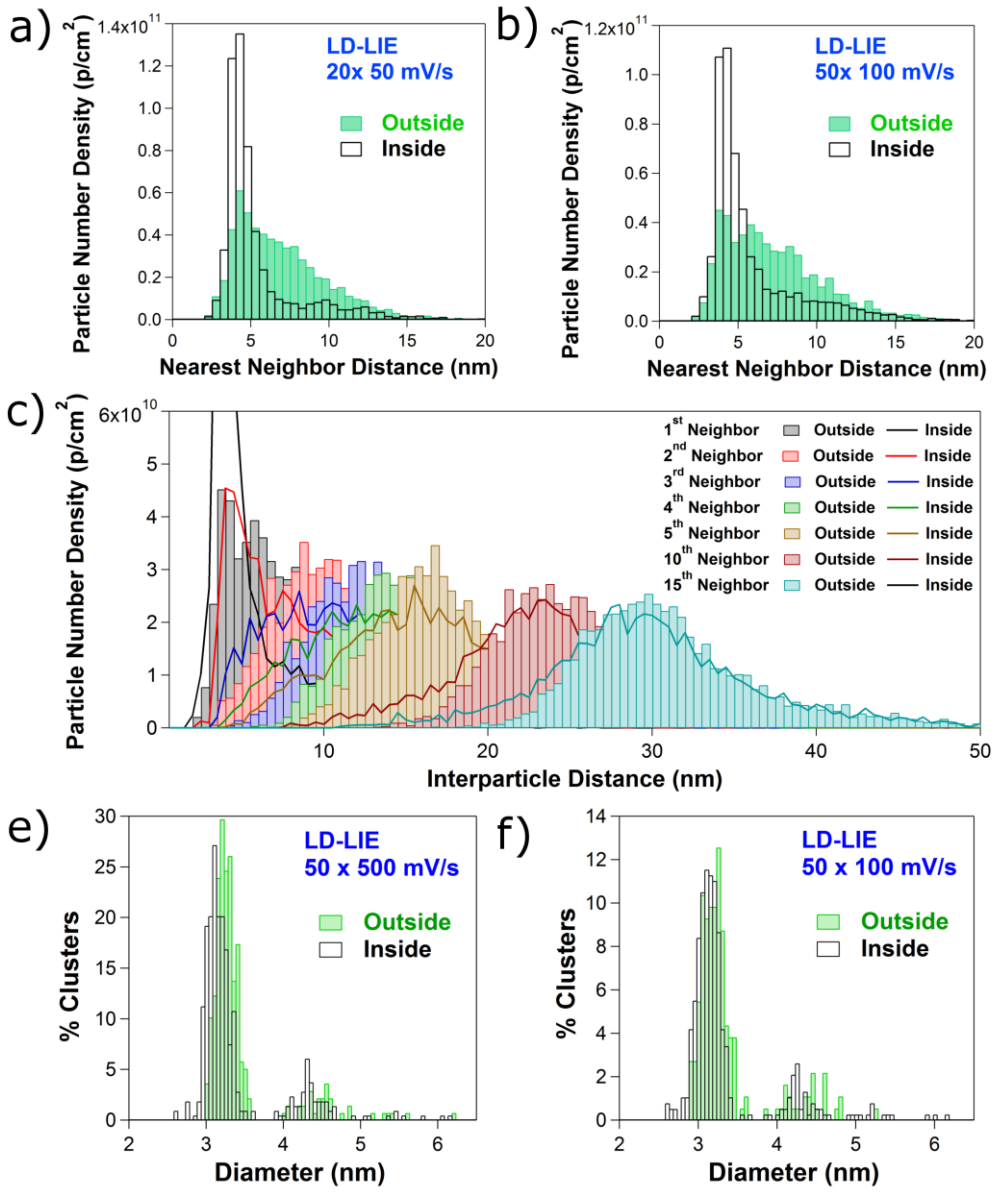

Figure 8 Nearest neighbor distance histograms before and after (a) 20 scans at 50 mV s^{-1} and (b) 50 scans at 100 mV s^{-1}. (e) Interparticle distance histograms for the 15 nearest neighbors before and after 50 scans at 100 mV s^{-1}. Pt NC size histograms before and after (e) 50 scans at 500 mV s^{-1} and (f) 50 scans at 100 mV s^{-1}.

The analysis of HAADF-STEM images after other series of cyclic voltammograms with different voltammetric scan rates (see Supporting Information Section S8, Figure S12) leads to the same conclusion: *NC re-arrangement within the LD-LIE sample occurs during ORR voltammetric experiments* and a larger extent of clustering is found for longer total polarization times. To be certain that the contact and release of the meniscus did not affect the stability of the Pt NCs for the LD-LIE sample, the same pipette was approached and left in meniscus contact with the CCTG for a similar time as for the voltammetric measurements reported, but without applying any potential. After removal of the meniscus, no changes in the NC distribution were observed.

The size distributions of the LD-LIE NCs before and after 50 scans at 500 mV s^{-1} and 50 scans at 100 mV s^{-1} are shown in figures 8e and 8f. These is a slight shift towards smaller sizes: the average NC diameter changes from 3.22 ± 0.12 nm to 3.11 ± 0.14 nm (e) and from 3.16 ± 0.15 to 3.09 ± 0.15 nm (f), indicating that a small extent of Pt dissolution may occur, but not to account for the significant decrease of electrochemical activity during ORR reported in Figure 3a. A summary of all parameters deduced from microscopy, before and after ORR experiments, is given in Supporting Information section S8, Table S7.

The high magnification images in Figure 7b, and the statistical evaluation of the number of singlets, doublets and larger clusters inside and adjacent to the areas probed by SECCM (Supporting Information, Section S7, Figure S11b), indicates that NCs are arranged into characteristic groups, but without aggregation. A similar arrangement has been observed previously for Pt NCs soft-landed on HOPG with lower impact energy (typically at 0.1 eV/atom).[102–104] Among reasons for this behavior,[102–104] NC patterns of this type have been attributed to the effect of small amounts of lightweight chemical species (probably CO[104]) that

readily adsorb on the Pt surface even under UHV conditions. In our case, the edge-to-edge distance between NCs is ca. 1.5 nm, close to the ~ 1.2 nm seen in UHV deposition studies. This further reinforces the idea, proposed above, that RIs generated during the ORR react with the carbon support, and as a consequence, a layer of carbon and oxygen containing reaction products adsorbs at the surface of the Pt NCs. This would, on the one hand, prevent the Pt NCs from sintering, and on the other hand, hinder the ORR at the poisoned surface, as observed.

Although STEM imaging cannot identify which species may be covering or poisoning the Pt surface, the brighter background in the STEM images of regions of the CCTGs where electrochemical measurements have been made (e.g. Figure 1c) is reminiscent of contamination build-up during STEM imaging, caused by the polymerisation of carbonaceous species induced by the electron beam.[105,106] It is tempting to speculate that the brighter background observed is caused by a similar process, but one induced by electrochemistry, in line with the XPS analysis presented earlier.

Nanocluster migration during ORR

The migration of weakly bound supported NCs during electrochemistry is an emerging phenomena that has been reported during electrodeposition[52–54,107,108] and other electrochemical processes,[50,109,110] but the physicochemical processes that drive this migration have not been analyzed in detail. The experimental SECCM setup (see Figure 1 and Figure 2a) does not presently allow the measurements to be done in oxygen-free electrolyte. Thus, although random (or directional) movement of the clusters caused by potential cycling alone (rather than by the ORR) cannot be disregarded, the fact that the degree of clustering seems to be dependent on the total

measurement time, rather than the voltammetric scan rate (Supporting Information, Figure S12) favors the idea that the movement is caused by the ORR.

Recently, it has been postulated that when a NP is weakly bound to a surface and an electrochemical reaction occurs non-uniformly at the NP surface, there is an electrochemical propulsion of the NP, resulting in its detachment from the surface.[111,112] Self-generated motion of nano-objects has been investigated for NPs, nanorods and microparticles in solution, with[113–116] and without[117–121] an applied external electric field. In essence, when different (i.e., bipolar) electrochemical reactions occur at the opposite sides of a nanoentity, gradients of ions and of other chemical species are generated. Two possibilities for driving NP motion have been considered: (i) the electrical field resulting from a gradient of ions drives the motion of the NPs by self-electrophoresis; (ii) gradients in the concentration of solute molecules generates fluid flow which results in the motion of the NPs in the opposite direction by self-diffusiophoresis.[119] In this regard, since local chemical gradients can also cause local surface tension gradients, Marangoni effects could locally drive the liquid from low to high surface tension, resulting in NP motion in the opposite direction.[117]

Although our studies concern monometallic Pt NCs, chemical concentration gradients of ions (protons), reactants (O_2 and protons) and reaction products (ROS) are generated because *the NCs are non-uniformly distributed on the support surface* and the flux of reactants (O_2 and protons) and products will be higher at those (parts of) NCs, which are less diffusionally coupled to (shielded from reactants by) neighboring NCs. This would result in non-uniform electric fields and/or chemical gradients which would tend to propel NCs towards each other (Figure 9).

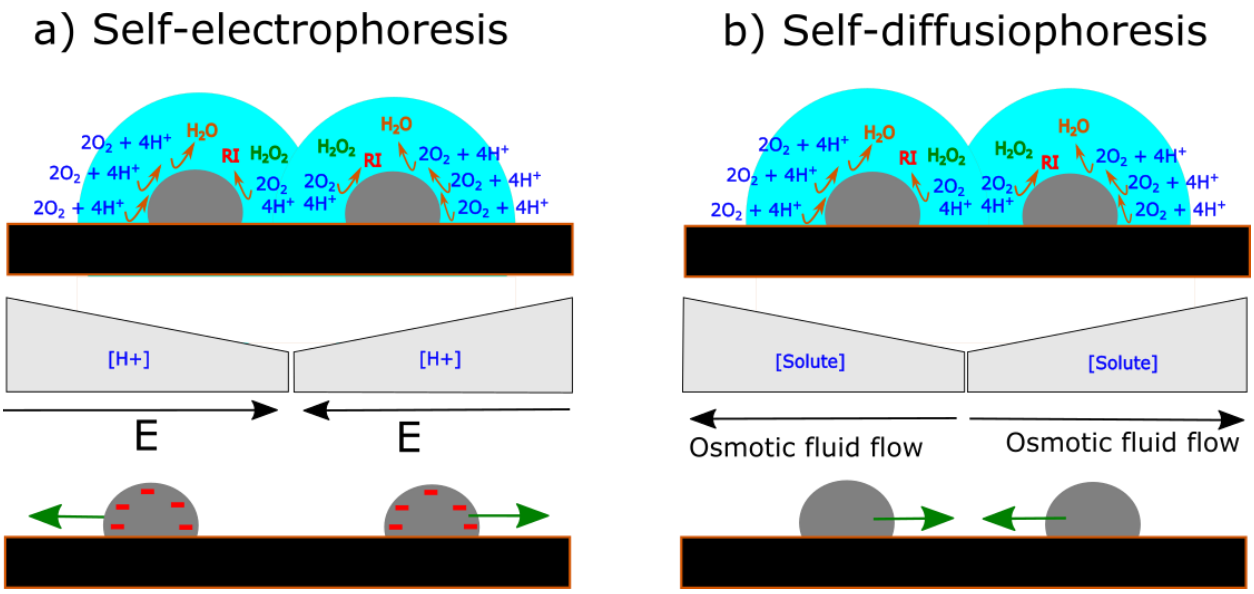

Figure 9 Schematic representation of two possible driving forces for NC migration due to non-uniform rates of ORR at different parts of Pt NCs as a result of different extents of diffusional shielding. a) Self-electrophoresis: a gradient of protons generates an electric field that would push the particles away from each other. b) Self-diffusiophoresis: the stoichiometry of the ORR would lead to a gradient of solute molecules that would drag the solvent through osmosis towards the diffusionally uncoupled region. This in turn would exert a force into the NCs in the opposite direction.

Although a self-electrophoretic mechanism (Figure 9a) could contribute to NC motion, the proton concentration will be lower at the coupled (shielded) parts of the NCs, leading to an electric field that would push the negatively charged Pt NCs away from each other, which is opposite to what is seen experimentally. Alternatively, a self-diffusiophoretic mechanism, which has also been shown to result in motility of colloids,[119] would be a more plausible driving force since it would propel the particles towards each other (Figure 9b).

FEM simulations were implemented to test the reasonableness of these arguments through a model which precisely represented the NC geometrical arrangement on the support surface. Full details of the simulations are presented in the Supporting Information, Section S9. Briefly, NC locations were extracted from TEM images taken from areas that were located immediately outside (Figures 10a and 10b) or inside (Figures 10d and 10e) the SECCM meniscus on the LD-LIE sample in order to precisely mimic the experimental arrangement of NCs. The NCs were electrochemically active, the support was inert, with reactant species, A (concentration 0.2 mM, similar to O_2 in aerated solution), undergoing simple diffusion-controlled electron transfer at the NCs.

From these simulations, flux maps could be extracted, as exemplified in Figures 10c and 10f. Due to the randomness of the NC distribution before any electrochemical measurement (Figures 10a, 10b and 10c), there is an inhomogeneous distribution of flux around different NCs. Zooming in on individual NCs in Figures 10g, 10h and 10i, it can be seen that this uneven distribution of flux around individual NCs is highly dependent on their clustering. Where NCs are shielded by neighboring NCs, a lower flux is seen whereas isolated particles exhibit more even distributions of higher flux. The flux distribution becomes more inhomogeneous when the particles move closer after the ORR measurements (Figures 10d, 10e and 10f).

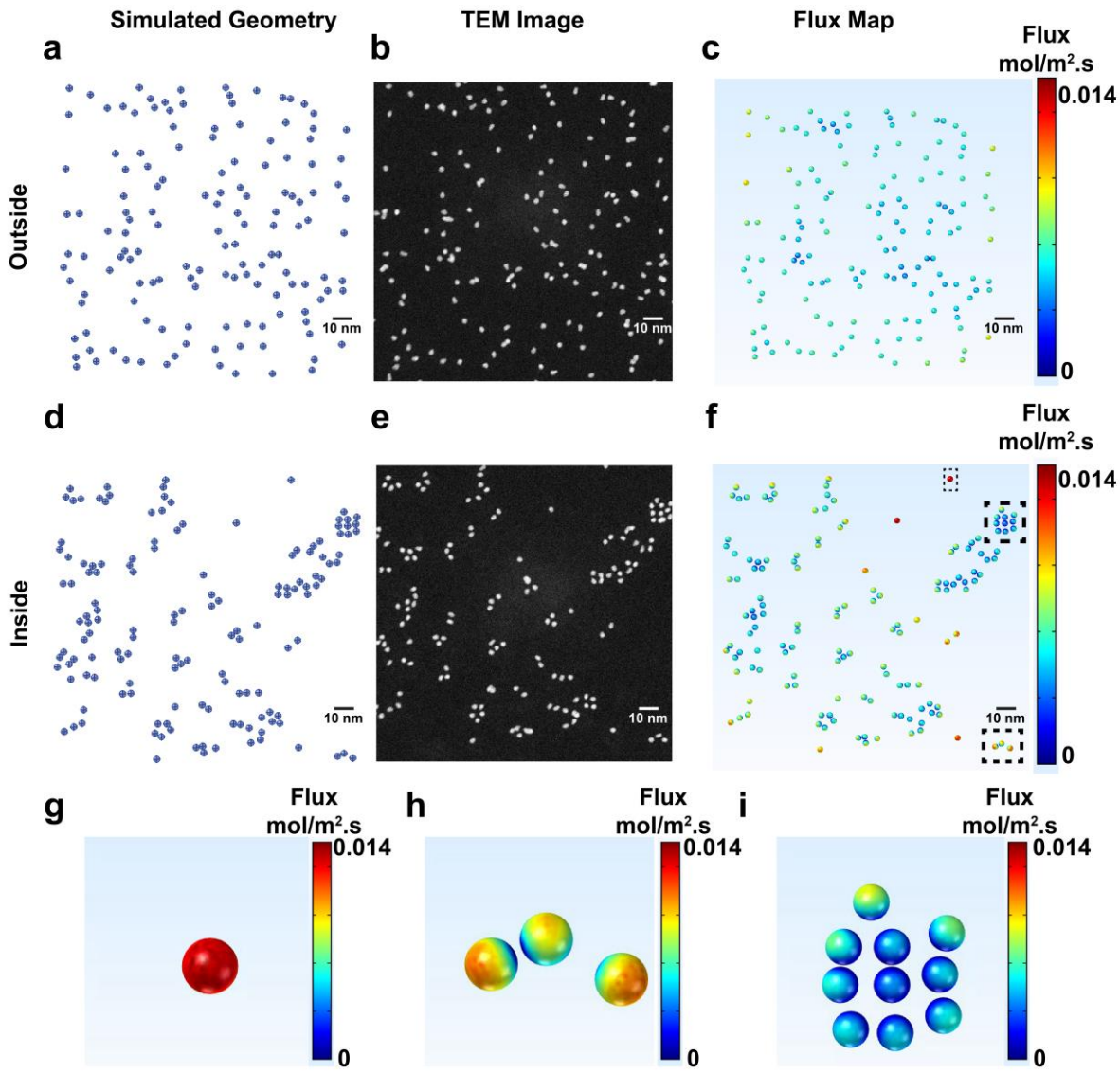

Figure 10 Simulated Pt NC positions (a,d) taken from STEM micrographs (b,e) in a region just outside (a-c) or at which SECCM measurements had been performed (d-f). Flux maps (c,f) extracted from FEM simulations,revealing an uneven distribution of flux around individual NPs. The fluxes at individual NCs highlighted in (f) are shown in (g-i).

Since re-arrangement of the Pt NCs could affect the electrochemical current measured for ORR, the effect of NC array formation on the expected electrochemical current was also explored. In

Supporting Information Section S9, a model array of 9 NPs with varying separation is considered, with a schematic of the simulation domain presented in Figure S14. As expected, as the NC separation becomes smaller, there is significant diffusional overlap between neighboring NCs. Analysis of the overall diffusion-limited current for the NC distributions typical of inside and outside the SECCM meniscus, presented in Figure 10, reveals only ca. 2% fall in the current following the change in NC arrangement between 'out' and 'in', and this cannot account for the significant decrease in electrochemical activity observed experimentally during voltammetric cycling such as presented in Figure 3. Thus, although NCs can move around on the surface, this would have little impact on the overall mass transport limited currents. The ORR is more complex, involving transient RIs, and the overall current will be more sensitive to the NC arrangement. While NC movement on the surface will contribute to some of the loss of activity seen for the ORR in NC arrays, the main factor responsible is poisoning of the surface, for which the NC density is particularly important.

CONCLUSIONS

We have presented an approach that allows electrocatalytic measurements of *a small number of well-defined and characterized NCs under high mass transport rates,* combined with high resolution HAADF-STEM imaging of a large fraction of the same NCs. The interpretation of electrochemical data combined with statistical analysis of high resolution STEM images and XPS characterization of the substrate surface, has provided major insights into the ORR mechanism at the nanoscale under conditions of low catalyst loading, high mass transport conditions and extended potential range, of relevance to PEMFC electrocatalysis.

Under the high mass transport conditions inherent in the SECCM setup, the ORR electrochemical response at Pt_{923} NCs ($d \approx 3$ nm) becomes limited by H adsorption at $E \leq 0.2$ V, and is strongly affected by the extent of voltammetric measurements are made, deteriorating with time, especially when the Pt surface coverage is low. Under these experimental conditions, particle detachment, Pt dissolution, Ostwald Ripening, NC migration, aggregation/sintering and H_2O_2 poisoning can all be excluded as major causes of the decrease of electrochemical activity during ORR cycling. Rather, XPS and HAADF-STEM analysis indicate that the decrease in activity is primarily related to the formation of carbon/oxygen groups (i.e., CO) that are generated by the reaction of reactive oxygen species, produced as intermediates, with the carbon support surface, that adsorb and poison the surface of the Pt NCs. The extent of this process depends on the Pt NC surface coverage, being most noticeable for low Pt NC coverages on the carbon support surface.

The deposition impact energy, i.e., adhesion of the Pt NCs to the carbon substrate, does not influence the ORR activity, but affects drastically the Pt NC stability on the carbon substrate. For the higher deposition impact energy employed in this work (1.6 eV/atom), the cluster geometrical arrangements are essentially identical before and after the electrochemical measurements. However, for the lower deposition impact energy (0.54 eV/atom), Pt NCs migrate during the ORR measurements and form characteristic arrangements on the surface, without aggregating, in groups of up to more than 15 NCs. With the support of FEM simulations, we postulate that such directional NC migration is caused by an uneven distribution of electrochemical flux around individual NPs caused by the initial random NC distribution across the surface, which generates non-uniform electric fields and/or chemical gradients.

METHODS

Cluster Synthesis Setup. Mass-selected Pt clusters were produced in a magnetron-sputtering, gas-aggregation cluster beam source with a lateral time-of-flight filter, as described in Supporting Information, Section S1 and elsewhere.[66,67] The substrate voltage was set to either 500 V (0.54 eV/atom) or 1500 V (1.6 eV/atom) during deposition.

HAADF-STEM. STEM images were recorded using a 200 kV JEOL JEM-2100F scanning transmission electron microscope with an incorporated spherical aberration corrector (CEOS GmbH) and using a high-angle annular dark field (HAADF) detector, operated with inner and outer collection angles of 62 and 164 mrad, respectively.

SECCM Setup and electrochemical measurements. The SECCM setup was presented in Figure 1 and the related discussion, and has been described in detail.[71] A dual-barrel borosilicate capillary (o.d. 1.5 mm, i.d. 1.2 mm, TGC 150-10, Harvard Apparatus) was pulled to generate a pipette with a tapered end of ~ 1 μm, using a CO_2-laser puller (P-2000, Sutter Instruments). Two palladium wires (saturated with H_2 by applying -3.0 V for 30 min in 0.1 M $HClO_4$) were placed into each barrel and used as QRCEs in all the electrochemical measurements. The pipette was mounted vertically on a *z*-piezoelectric positioner (P-753.1CD LISA, PhysikInstrumente), over the substrate (Pt-loaded TEM grid) and the coarse and fine approaches of pipette towards the substrate were conducted with control of a picomotor (Newport, 8303 Picomotor Actuator) and the *z*-piezoelectric positioner, respectively. A data acquisition rate of *ca.* 390 points/s (each point the average of 256 readings) was achieved by use of an FPGA card (PCIe-7852R) with a LabVIEW 2013 (National Instruments) interface. With reference to Figure 1, the meniscus was landed on the CCTG surface, without physical contact from the pipette probe itself, by monitoring the surface

current at the substrate (arising from double layer charging). The electrolyte was air-saturated 0.1 M $HClO_4$ aqueous solution. Pd-H_2 wires were used as QRCEs in all the electrochemical measurements. The H_2O_2 measurements were performed with identical conditions, except that the solutions (0.1 M $HClO_4$) included contained 1 or 5 mM H_2O_2.

XPS Characterization. For XPS characterization, the TEM grids with Pt NCs were immersed in a 0.1 M solution of $HClO_4$ and 200 CV scans were performed from 1.1 V to 0.05 V vs Pd-H_2 reference electrode, with a scan rate of 200 mV s^{-1}, using a commercial bipotentiostat (730A, CH Instruments,inc., Austin, USA). The grids were then mounted on to a metallic sample bar using electrically-conductive carbon tape and loaded in to a Kratos Axis Ultra DLD spectrometer. XPS measurements were performed in a pressure below 1 x 10^{-9} mbar with the sample illuminated using an Al k_α monochromated x-ray source. The binding energy scale and the transmission function of the spectrometer were calibrated using clean Ag foil prior to the experiments commencing. Survey spectra were acquired using a pass energy of 160 eV while high resolution core level spectra were acquired at a pass energy of 20 eV (resolution approx. 0.4 eV). All measurements were performed using an analysis area 110 μm in diameter. Data were analysed using CasaXPS, employing Voigt lineshapes for all peaks except the metallic Pt contributions to the Pt 4f region where an asymmetric Lorentzian lineshape, LA(1.5,90,30), was used

Finite Element Simulations. FEM simulations were performed in COMSOL Multiphysics 5.2a with the transport of diluted species module. For full details, please see Supporting Information, Section S9 and the main text.

Supporting Information Available: Cluster deposition setup and procedure. Cluster characterization before electrochemical measurements: Effect of the substrate voltage on the cluster shape and size distribution. ORR measurements with added H2O2. XPS Analysis. HAADF-STEM analysis for the LD-HIE sample. Analysis of the singlets, doublets and larger particles for the LD-HIE, LD-LIE and HD-HIE samples. HAADF-STEM analysis for the LD-LIE sample. FEM Simulations: effect of Clustering on Electrochemical Response. This material is available free of charge via the Internet at http://pubs.acs.org.

Corresponding Authors

* Jon Ustarroz, jon.ustarroz@vub.be

* Patrick R. Unwin, P.R.Unwin@warwick.ac.uk

Author Contributions

The manuscript was written through contributions of all authors. All authors have given approval to the final version of the manuscript.

Funding Sources

J.U. was supported by the Fonds Wetenschappelijk Onderzoek (FWO) in Flanders (postdoctoral grant 12I7816N). I.M.O. was supported by EPSRC, Birmingham Science City. P.R.U. thanks the Royal Society for a Wolfson Research Merit Award. D.P. was supported by the Leverhulme Trust and G.Z. and M.K. by University of Warwick Chancellor's International Scholarships.

Notes

ACKNOWLEDGMENT

J.U. acknowledges funding from the Fonds Wetenschappelijk Onderzoek (FWO) in Flanders (postdoctoral grant 12I7816N). P.R.U. thanks the Royal Society for a Wolfson Research Merit Award. The STEM instrument used in this research was obtained through the Birmingham Science City project "Creating and Characterising Next Generation Advanced Materials", supported by Advantage West Midlands (AWM) and partly funded by the European Regional Development Fund (ERDF). D.P. was supported by the Leverhulme Trust and G.Z. and M.K. by University of Warwick Chancellor's International Scholarships.

REFERENCES

(1) Nesselberger, M.; Ashton, S.; Meier, J. C.; Katsounaros, I.; Mayrhofer, K. J. J.; Arenz, M. The Particle Size Effect on the Oxygen Reduction Reaction Activity of Pt Catalysts: Influence of Electrolyte and Relation to Single Crystal Models. *J. Am. Chem. Soc.* **2011**, *133* (43), 17428–17433.

(2) Gómez-Marín, A. M.; Rizo, R.; Feliu, J. M. Oxygen Reduction Reaction at Pt Single Crystals: A Critical Overview. *Catal. Sci. Technol.* **2014**, *4* (6), 1685.

(3) Katsounaros, I.; Cherevko, S.; Zeradjanin, A. R.; Mayrhofer, K. J. J. Oxygen Electrochemistry as a Cornerstone for Sustainable Energy Conversion. *Angew. Chemie - Int. Ed.* **2014**, *53* (1), 102–121.

(4) Crooks, R. M. Concluding Remarks: Single Entity Electrochemistry One Step at a Time. *Faraday Discuss.* **2016**, *193*, 533–547.

(5) Gómez-Marín, A. M.; Rizo, R.; Feliu, J. M. Some Reflections on the Understanding of the Oxygen Reduction Reaction at Pt(111). *Beilstein J. Nanotechnol.* **2013**, *4* (1), 956–967.

(6) Kuzume, A.; Herrero, E.; Feliu, J. M. Oxygen Reduction on Stepped Platinum Surfaces in Acidic Media. *J. Electroanal. Chem.* **2007**, *599* (2), 333–343.

(7) Nesselberger, M.; Roefzaad, M.; Fayçal Hamou, R.; Ulrich Biedermann, P.; Schweinberger, F. F.; Kunz, S.; Schloegl, K.; Wiberg, G. K. H.; Ashton, S.; Heiz, U.; et al. The Effect of Particle Proximity on the Oxygen Reduction Rate of Size-Selected Platinum Clusters. *Nat. Mater.* **2013**, *12* (10), 919–924.

(8) Choi, C. H.; Kim, M.; Kwon, H. C.; Cho, S. J.; Yun, S.; Kim, H.-T.; Mayrhofer, K. J. J.;

Kim, H.; Choi, M. Tuning Selectivity of Electrochemical Reactions by Atomically Dispersed Platinum Catalyst. *Nat. Commun.* **2016**, *7* (Iek 11), 10922.

(9) Fabbri, E.; Taylor, S.; Rabis, A.; Levecque, P.; Conrad, O.; Kötz, R.; Schmidt, T. J. The Effect of Platinum Nanoparticle Distribution on Oxygen Electroreduction Activity and Selectivity. *ChemCatChem* **2014**, *6* (5), 1410–1418.

(10) Von Weber, A.; Baxter, E. T.; White, H. S.; Anderson, S. L. Cluster Size Controls Branching between Water and Hydrogen Peroxide Production in Electrochemical Oxygen Reduction at Pt N /ITO. *J. Phys. Chem. C* **2015**, *119* (20), 11160–11170.

(11) Taylor, S.; Fabbri, E.; Levecque, P.; Schmidt, T. J.; Conrad, O. The Effect of Platinum Loading and Surface Morphology on Oxygen Reduction Activity. *Electrocatalysis* **2016**, *7* (4), 287–296.

(12) Mistry, H.; Behafarid, F.; Reske, R.; Varela, A. S.; Strasser, P.; Roldan Cuenya, B. Tuning Catalytic Selectivity at the Mesoscale via Interparticle Interactions. *ACS Catal.* **2016**, *6* (2), 1075–1080.

(13) Mistry, H.; Varela, A. S.; Kühl, S.; Strasser, P.; Cuenya, B. R. Nanostructured Electrocatalysts with Tunable Activity and Selectivity. *Nat. Rev. Mater.* **2016**, *1* (4), 16009.

(14) Antolini, E. Structural Parameters of Supported Fuel Cell Catalysts: The Effect of Particle Size, Inter-Particle Distance and Metal Loading on Catalytic Activity and Fuel Cell Performance. *Appl. Catal. B Environ.* **2016**, *181*, 298–313.

(15) Paulus, U. A.; Schmidt, T. J.; Gasteiger, H. A.; Behm, R. J. Oxygen Reduction on a High-Surface Area Pt/Vulcan Carbon Catalyst: A Thin-Film Rotating Ring-Disk Electrode Study.

J. Electroanal. Chem. **2001**, *495* (2), 134–145.

(16) Gasteiger, H. A.; Kocha, S. S.; Sompalli, B.; Wagner, F. T. Activity Benchmarks and Requirements for Pt, Pt-Alloy, and Non-Pt Oxygen Reduction Catalysts for PEMFCs. *Appl. Catal. B Environ.* **2005**, *56* (1–2), 9–35.

(17) Pedersen, C. M.; Escudero-Escribano, M.; Velázquez-Palenzuela, A.; Christensen, L. H.; Chorkendorff, I.; Stephens, I. E. L. Benchmarking Pt-Based Electrocatalysts for Low Temperature Fuel Cell Reactions with the Rotating Disk Electrode: Oxygen Reduction and Hydrogen Oxidation in the Presence of CO (Review Article). *Electrochim. Acta* **2015**, *179*, 647–657.

(18) Speder, J.; Spanos, I.; Zana, A.; Kirkensgaard, J. J. K.; Mortensen, K.; Altmann, L.; Bäumer, M.; Arenz, M. From Single Crystal Model Catalysts to Systematic Studies of Supported Nanoparticles. *Surf. Sci.* **2015**, *631*, 278–284.

(19) Mayrhofer, K. J. J.; Strmcnik, D.; Blizanac, B. B.; Stamenkovic, V. R.; Arenz, M.; Markovic, N. M. Measurement of Oxygen Reduction Activities via the Rotating Disc Electrode Method: From Pt Model Surfaces to Carbon-Supported High Surface Area Catalysts. *Electrochim. Acta* **2008**, *53* (7), 3181–3188.

(20) Yu, Y.; Sun, Q.; Liu, X.; Wu, H.; Zhou, T.; Shi, G. Size-Controllable Gold-Platinum Alloy Nanoparticles on Nine Functionalized Ionic-Liquid Surfaces and Their Application as Electrocatalysts for Hydrogen Peroxide Reduction. *Chem. Eur. J.* **2011**, *17* (40), 11314–11323.

(21) Meier, J. C.; Galeano, C.; Katsounaros, I.; Witte, J.; Bongard, H. J.; Topalov, A. a;

Baldizzone, C.; Mezzavilla, S.; Schüth, F.; Mayrhofer, K. J. J. Design Criteria for Stable Pt/C Fuel Cell Catalysts. *Beilstein J. Nanotechnol.* **2014**, *5*, 44–67.

(22) Lee, H.; Habas, S. E.; Kweskin, S.; Butcher, D.; Somorjai, G. A.; Yang, P. Morphological Control of Catalytically Active Platinum Nanocrystals. *Angew. Chemie - Int. Ed.* **2006**, *45* (46), 7824–7828.

(23) Seidel, Y. E.; Schneider, A.; Jusys, Z.; Wickman, B.; Kasemo, B.; Behm, R. J. Mesoscopic Mass Transport Effects in Electrocatalytic Processes. *Faraday Discuss.* **2008**, *140*, 167–184.

(24) Chen, S.; Kucernak, A. Electrocatalysis under Conditions of High Mass Transport Rate: Oxygen Reduction on Single Submicrometer-Sized Pt Particles Supported on Carbon. *J. Phys. Chem. B* **2004**, *108* (10), 3262–3276.

(25) Proch, S.; Wirth, M.; White, H. S.; Anderson, S. L. Strong Effects of Cluster Size and Air Exposure on Oxygen Reduction and Carbon Oxidation Electrocatalysis by Size-Selected Ptn (N < 11) on Glassy Carbon Electrodes. *J. Am. Chem. Soc.* **2013**, *135* (8), 3073–3086.

(26) Dumitrescu, I.; Crooks, R. M. Effect of Mass Transfer on the Oxygen Reduction Reaction Catalyzed by Platinum Dendrimer Encapsulated Nanoparticles. *Proc. Natl. Acad. Sci.* **2012**, *109* (29), 11493–11497.

(27) Schneider, A.; Colmenares, L.; Seidel, Y. E.; Jusys, Z.; Wickman, B.; Kasemo, B.; Behm, R. J. Transport Effects in the Oxygen Reduction Reaction on Nanostructured, Planar Glassy Carbon Supported Pt/GC Model Electrodes. *Phys. Chem. Chem. Phys.* **2008**, *10* (14), 1931.

(28) Yang, H.; Kumar, S.; Zou, S. Electroreduction of O2 on Uniform Arrays of Pt

Nanoparticles. *J. Electroanal. Chem.* **2013**, *688*, 180–188.

(29) Hodnik, N.; Dehm, G.; Mayrhofer, K. J. J. Importance and Challenges of Electrochemical in Situ Liquid Cell Electron Microscopy for Energy Conversion Research. *Acc. Chem. Res.* **2016**, *49* (9), 2015–2022.

(30) Holtz, M. E.; Yu, Y.; Gunceler, D.; Gao, J.; Sundararaman, R.; Schwarz, K. A.; Arias, T. A.; Abruña, H. D.; Muller, D. A. Nanoscale Imaging of Lithium Ion Distribution during in Situ Operation of Battery Electrode and Electrolyte. *Nano Lett.* **2014**, *14*, 1453–1459.

(31) Smith, M. C.; Gilbert, J. A.; Mawdsley, J. R.; Seifert, S.; Myers, D. J. In Situ Small-Angle X-Ray Scattering Observation of Pt Catalyst Particle Growth during Potential Cycling. *J. Am. Chem. Soc.* **2008**, *130* (26), 8112–8113.

(32) Lopez-Haro, M.; Dubau, L.; Guétaz, L.; Bayle-Guillemaud, P.; Chatenet, M.; André, J.; Caqué, N.; Rossinot, E.; Maillard, F. Atomic-Scale Structure and Composition of Pt3Co/C Nanocrystallites during Real PEMFC Operation: A STEM-EELS Study. *Appl. Catal. B Environ.* **2014**, *152–153* (1), 300–308.

(33) Yu, Y.; Xin, H. L.; Hovden, R.; Wang, D.; Rus, E. D.; Mundy, J. A.; Muller, D. A.; Abruña, H. D. Three-Dimensional Tracking and Visualization of Hundreds of Pt-Co Fuel Cell Nanocatalysts during Electrochemical Aging. *Nano Lett.* **2012**, *12* (9), 4417–4423.

(34) Goris, B.; Bals, S.; Van den Broek, W.; Carbó-Argibay, E.; Gómez-Graña, S.; Liz-Marzán, L. M.; Van Tendeloo, G. Atomic-Scale Determination of Surface Facets in Gold Nanorods. *Nat. Mater.* **2012**, *11* (11), 930–935.

(35) Bals, S.; Goris, B.; Liz-Marzán, L. M.; Van Tendeloo, G. Three-Dimensional

Characterization of Noble-Metal Nanoparticles and Their Assemblies by Electron Tomography. *Angew. Chemie - Int. Ed.* **2014**, *53* (40), 10600–10610.

(36) Dubau, L.; Castanheira, L.; Berthomé, G.; Maillard, F. An Identical-Location Transmission Electron Microscopy Study on the Degradation of Pt/C Nanoparticles under Oxidizing, Reducing and Neutral Atmosphere. *Electrochim. Acta* **2013**, *110*, 273–281.

(37) Dubau, L.; Castanheira, L.; Maillard, F.; Chatenet, M.; Lottin, O.; Maranzana, G.; Dillet, J.; Lamibrac, A.; Perrin, J. C.; Moukheiber, E.; et al. A Review of PEM Fuel Cell Durability: Materials Degradation, Local Heterogeneities of Aging and Possible Mitigation Strategies. *Wiley Interdiscip. Rev. Energy Environ.* **2014**, *3* (6), 540–560.

(38) Zadick, A.; Dubau, L.; Sergent, N.; Berthomé, G.; Chatenet, M. Huge Instability of Pt/C Catalysts in Alkaline Medium. *ACS Catal.* **2015**, *5* (8), 4819–4824.

(39) Arenz, M.; Zana, A. Fuel Cell Catalyst Degradation: Identical Location Electron Microscopy and Related Methods. *Nano Energy* **2015**, 1–15.

(40) Perez-Alonso, F. J.; Elkjær, C. F.; Shim, S. S.; Abrams, B. L.; Stephens, I. E. L.; Chorkendorff, I. B. Identical Locations Transmission Electron Microscopy Study of Pt/C Electrocatalyst Degradation during Oxygen Reduction Reaction. *J. Power Sources* **2011**, *196* (15), 6085–6091.

(41) Arán-Ais, R. M.; Yu, Y.; Hovden, R.; Solla-Gullón, J.; Herrero, E.; Feliu, J. M.; Abruña, H. D. Identical Location Transmission Electron Microscopy Imaging of Site-Selective Pt Nanocatalysts: Electrochemical Activation and Surface Disordering. *J. Am. Chem. Soc.* **2015**, *137* (47), 14992–14998.

(42) Shao-Horn, Y.; Sheng, W. C.; Chen, S.; Ferreira, P. J.; Holby, E. F.; Morgan, D. Instability of Supported Platinum Nanoparticles in Low-Temperature Fuel Cells. *Top. Catal.* **2007**, *46* (3–4), 285–305.

(43) Hartl, K.; Hanzlik, M.; Arenz, M. IL-TEM Investigations on the Degradation Mechanism of Pt/C Electrocatalysts with Different Carbon Supports. *Energy Environ. Sci.* **2011**, *4* (1), 234–238.

(44) Meier, J. C.; Katsounaros, I.; Galeano, C.; Bongard, H. J.; Topalov, A. A.; Kostka, A.; Karschin, A.; Schüth, F.; Mayrhofer, K. J. J. Stability Investigations of Electrocatalysts on the Nanoscale. *Energy Environ. Sci.* **2012**, *5* (11), 9319.

(45) Schlögl, K.; Hanzlik, M.; Arenz, M. Comparative IL-TEM Study Concerning the Degradation of Carbon Supported Pt-Based Electrocatalysts. *J. Electrochem. Soc.* **2012**, *159* (6), B677.

(46) Schlögl, K.; Mayrhofer, K. J. J.; Hanzlik, M.; Arenz, M. Identical-Location TEM Investigations of Pt/C Electrocatalyst Degradation at Elevated Temperatures. *J. Electroanal. Chem.* **2011**, *662* (2), 355–360.

(47) Wang, F.; Li, C.; Sun, L.-D.; Xu, C.-H.; Wang, J.; Yu, J. C.; Yan, C.-H. Porous Single-Crystalline Palladium Nanoparticles with High Catalytic Activities. *Angew. Chemie - Int. Ed.* **2012**, *51* (20), 4872–4876.

(48) Castanheira, L.; Dubau, L.; Maillard, F. Accelerated Stress Tests of Pt/HSAC Electrocatalysts: An Identical-Location Transmission Electron Microscopy Study on the Influence of Intermediate Characterizations. *Electrocatalysis* **2014**, *5* (2), 125–135.

(49) Nikkuni, F. R.; Vion-Dury, B.; Dubau, L.; Maillard, F.; Ticianelli, E. a.; Chatenet, M. The Role of Water in the Degradation of Pt3Co/C Nanoparticles: An Identical Location Transmission Electron Microscopy Study in Polymer Electrolyte Environment. *Appl. Catal. B Environ.* **2014**, *156–157*, 301–306.

(50) Hartl, K.; Nesselberger, M.; Mayrhofer, K. J. J.; Kunz, S.; Schweinberger, F. F.; Kwon, G.; Hanzlik, M.; Heiz, U.; Arenz, M. Electrochemically Induced Nanocluster Migration. *Electrochim. Acta* **2010**, *56* (2), 810–816.

(51) Ustarroz, J.; Gupta, U.; Hubin, A.; Bals, S.; Terryn, H. Electrodeposition of Ag Nanoparticles onto Carbon Coated TEM Grids: A Direct Approach to Study Early Stages of Nucleation. *Electrochem. Commun.* **2010**, *12* (12), 1706–1709.

(52) Ustarroz, J.; Ke, X.; Hubin, A.; Bals, S.; Terryn, H. New Insights into the Early Stages of Nanoparticle Electrodeposition. *J. Phys. Chem. C* **2012**, *116* (3), 2322–2329.

(53) Ustarroz, J.; Altantzis, T.; Hammons, J. a.; Hubin, A.; Bals, S.; Terryn, H. The Role of Nanocluster Aggregation, Coalescence, and Recrystallization in the Electrochemical Deposition of Platinum Nanostructures. *Chem. Mater.* **2014**, *26* (7), 2396–2406.

(54) Ustarroz, J.; Hammons, J. A.; Altantzis, T.; Hubin, A.; Bals, S.; Terryn, H. A Generalized Electrochemical Aggregative Growth Mechanism. *J. Am. Chem. Soc.* **2013**, *135*, 11550–11561.

(55) Percival, S. J.; Zhang, B. Electrocatalytic Reduction of Oxygen at Single Platinum Nanowires. *J. Phys. Chem. C* **2013**, *117* (27), 13928–13935.

(56) Clausmeyer, J.; Schuhmann, W. Nanoelectrodes: Applications in Electrocatalysis, Single-

Cell Analysis and High-Resolution Electrochemical Imaging. *TrAC - Trends Anal. Chem.* **2016**, *79*, 46–59.

(57) Byers, J. C.; Güell, A. G.; Unwin, P. R. Nanoscale Electrocatalysis: Visualizing Oxygen Reduction at Pristine, Kinked, and Oxidized Sites on Individual Carbon Nanotubes. *J. Am. Chem. Soc.* **2014**, *136* (32), 11252–11255.

(58) Kim, J.; Renault, C.; Nioradze, N.; Arroyo-Currás, N.; Leonard, K. C.; Bard, A. J. Electrocatalytic Activity of Individual Pt Nanoparticles Studied by Nanoscale Scanning Electrochemical Microscopy. *J. Am. Chem. Soc.* **2016**, *138* (27), 8560–8568.

(59) Kang, M.; Perry, D.; Bentley, C. L.; West, G.; Page, A.; Unwin, P. R. Simultaneous Topography and Reaction Flux Mapping at and around Electrocatalytic Nanoparticles. *ACS Nano* **2017**, *11* (9), 9525–9535.

(60) Xiao, X.; Bard, A. J. Observing Single Nanoparticle Collisions at an Ultramicroelectrode by Electrocatalytic Amplification. *J. Am. Chem. Soc.* **2007**, *129* (31), 9610–9612.

(61) Kleijn, S. E. F.; Lai, S. C. S.; Miller, T. S.; Yanson, A. I.; Koper, M. T. M.; Unwin, P. R. Landing and Catalytic Characterization of Individual Nanoparticles on Electrode Surfaces. *J. Am. Chem. Soc.* **2012**, *134*, 18558–18561.

(62) McKelvey, K.; German, S. R.; Zhang, Y.; White, H. S.; Edwards, M. A. Nanopipettes as a Tool for Single Nanoparticle Electrochemistry. *Curr. Opin. Electrochem.* **2017**, *6* (1), 4–9.

(63) Kucernak, A. R.; Toyoda, E. Studying the Oxygen Reduction and Hydrogen Oxidation Reactions under Realistic Fuel Cell Conditions. *Electrochem. Commun.* **2008**, *10* (11), 1728–1731.

(64) Zalitis, C. M.; Kramer, D.; Kucernak, A. R. Electrocatalytic Performance of Fuel Cell Reactions at Low Catalyst Loading and High Mass Transport. *Phys. Chem. Chem. Phys.* **2013**, *15* (12), 4329–4340.

(65) Anderson, M. J.; Ostojic, N.; Crooks, R. M. Microelectrochemical Flow Cell for Studying Electrocatalytic Reactions on Oxide-Coated Electrodes. *Anal. Chem.* **2017**, *89* (20), 11027–11035.

(66) von Issendorff, B.; Palmer, R. E. A New High Transmission Infinite Range Mass Selector for Cluster and Nanoparticle Beams. *Rev. Sci. Instrum.* **1999**, *70* (12), 4497–4501.

(67) Pratontep, S.; Carroll, S. J.; Xirouchaki, C.; Streun, M.; Palmer, R. E. Size-Selected Cluster Beam Source Based on Radio Frequency Magnetron Plasma Sputtering and Gas Condensation. *Rev. Sci. Instrum.* **2005**, *76* (4), 45103.

(68) Popok, V. N.; Barke, I.; Campbell, E. E. B.; Meiwes-Broer, K.-H. Cluster–surface Interaction: From Soft Landing to Implantation. *Surf. Sci. Rep.* **2011**, *66* (10), 347–377.

(69) Kang, M.; Momotenko, D.; Page, A.; Perry, D.; Unwin, P. R. Frontiers in Nanoscale Electrochemical Imaging: Faster, Multifunctional, and Ultrasensitive. *Langmuir* **2016**, *32* (32), 7993–8008.

(70) Güell, A. G.; Cuharuc, A. S.; Kim, Y. R.; Zhang, G.; Tan, S. Y.; Ebejer, N.; Unwin, P. R. Redox-Dependent Spatially Resolved Electrochemistry at Graphene and Graphite Step Edges. *ACS Nano* **2015**, *9* (4), 3558–3571.

(71) Zhang, G.; Guell, A. G.; Kirkman, P. M.; Lazenby, R. A.; Miller, T. S.; Unwin, P. R. Versatile Polymer-Free Graphene Transfer Method and Applications. *ACS Appl. Mater.*

Interfaces **2016**, *8* (12), 8008–8016.

(72) Chen, C.-H.; Meadows, K. E.; Cuharuc, A.; Lai, S. C. S.; Unwin, P. R. High Resolution Mapping of Oxygen Reduction Reaction Kinetics at Polycrystalline Platinum Electrodes. *Phys. Chem. Chem. Phys.* **2014**, *16* (34), 18545–18552.

(73) Markovic, N. M.; Gasteiger, H. A.; Ross, P. N. Oxygen Reduction on Platinum Low-Index Single-Crystal Surfaces in Sulfuric Acid Solution: Rotating Ring-Pt(hkl) Disk Studies. *J. Phys. Chem.* **1995**, *99* (11), 3411–3415.

(74) Gómez-Marín, A. M.; Schouten, K. J. P.; Koper, M. T. M.; Feliu, J. M. Interaction of Hydrogen Peroxide with a Pt(111) Electrode. *Electrochem. Commun.* **2012**, *22* (1), 153–156.

(75) Gómez-Marín, A. M.; Feliu, J. M. New Insights into the Oxygen Reduction Reaction Mechanism on Pt (111): A Detailed Electrochemical Study. *ChemSusChem* **2013**, *6* (6), 1091–1100.

(76) Gómez–Marín, A. M.; Feliu, J. M. Role of Oxygen-Containing Species at Pt(111) on the Oxygen Reduction Reaction in Acid Media. *J. Solid State Electrochem.* **2015**, *19* (9), 2831–2841.

(77) Eslamibidgoli, M. J.; Eikerling, M. H. Electrochemical Formation of Reactive Oxygen Species at Pt (111)-A Density Functional Theory Study. *ACS Catal.* **2015**, *5* (10), 6090–6098.

(78) Zhang, S.; Yuan, X.-Z.; Hin, J. N. C.; Wang, H.; Friedrich, K. A.; Schulze, M. A Review of Platinum-Based Catalyst Layer Degradation in Proton Exchange Membrane Fuel Cells.

J. Power Sources **2009**, *194* (2), 588–600.

(79) Hung, C.-C.; Lim, P.-Y.; Chen, J.-R.; Shih, H. C. Corrosion of Carbon Support for PEM Fuel Cells by Electrochemical Quartz Crystal Microbalance. *J. Power Sources* **2011**, *196* (1), 140–146.

(80) Kangasniemi, K. H.; Condit, D. A.; Jarvi, T. D. Characterization of Vulcan Electrochemically Oxidized under Simulated PEM Fuel Cell Conditions. *J. Electrochem. Soc.* **2004**, *151* (4), E125.

(81) Willsau, J.; Heitbaum, J. The Influence of Pt-Activation on the Corrosion of Carbon in Gas Diffusion Electrodes-A Dems Study. *J. Electroanal. Chem.* **1984**, *161* (1), 93–101.

(82) Li, W.; Lane, A. M. Investigation of Pt Catalytic Effects on Carbon Support Corrosion of the Cathode Catalyst in PEM Fuel Cells Using DEMS Spectra. *Electrochem. Commun.* **2009**, *11* (6), 1187–1190.

(83) Rapecki, T.; Nowicka, A. M.; Donten, M.; Scholz, F.; Stojek, Z. Activity Changes of Glassy Carbon Electrodes Caused by Their Exposure to OH• Radicals. *Electrochem. Commun.* **2010**, *12* (11), 1531–1534.

(84) Maass, S.; Finsterwalder, F.; Frank, G.; Hartmann, R.; Merten, C. Carbon Support Oxidation in PEM Fuel Cell Cathodes. *J. Power Sources* **2008**, *176* (2), 444–451.

(85) Kinoshita, K. *Carbon: Electrochemical and Physicochemical Properties*; Wiley & Sons: New York, 1988.

(86) Cai, M.; Ruthkosky, M. S.; Merzougui, B.; Swathirajan, S.; Balogh, M. P.; Oh, S. H. Investigation of Thermal and Electrochemical Degradation of Fuel Cell Catalysts. *J. Power*

Sources **2006**, *160* (2), 977–986.

(87) Peng, Z.; Chen, Y.; Bruce, P. G.; Xu, Y. Direct Detection of the Superoxide Anion as a Stable Intermediate in the Electroreduction of Oxygen in a Non-Aqueous Electrolyte Containing Phenol as a Proton Source. *Angew. Chemie - Int. Ed.* **2015**, *54* (28), 8165–8168.

(88) Li, X.; Gewirth, A. A. Oxygen Electroreduction through a Superoxide Intermediate on Bi-Modified Au Surfaces. *J. Am. Chem. Soc.* **2005**, *127* (14), 5252–5260.

(89) Shao, M.; Liu, P.; Adzic, R. R. Superoxide Anion Is the Intermediate in the Oxygen Reduction Reaction on Platinum Electrodes. *J. Am. Chem. Soc.* **2006**, *128* (23), 7408–7409.

(90) Zhang, C.; Fan, F. F.; Bard, A. J. Electrochemistry of Oxygen in Concentrated NaOH Solutions: Solubility, Diffusion Coefficients, and Superoxide Formation. *J. Am. Chem. Soc.* **2009**, *131* (1), 177–181.

(91) Ohguri, N.; Nosaka, A. Y.; Nosaka, Y. Detection of OH Radicals as the Effect of Pt Particles in the Membrane of Polymer Electrolyte Fuel Cells. *J. Power Sources* **2010**, *195* (15), 4647–4652.

(92) Noël, J. M.; Latus, A.; Lagrost, C.; Volanschi, E.; Hapiot, P. Evidence for OH Radical Production during Electrocatalysis of Oxygen Reduction on Pt Surfaces: Consequences and Application. *J. Am. Chem. Soc.* **2012**, *134* (5), 2835–2841.

(93) Noël, J. M.; Yu, Y.; Mirkin, M. V. Dissolution of Pt at Moderately Negative Potentials during Oxygen Reduction in Water and Organic Media. *Langmuir* **2013**, *29* (5), 1346–1350.

(94) Shao, M. H.; Adzic, R. R. Spectroscopic Identification of the Reaction Intermediates in Oxygen Reduction on Gold in Alkaline Solutions. *J. Phys. Chem. B* **2005**, *109* (35), 16563–

16566.

(95) Panchenko, A.; Dilger, H.; Kerres, J.; Hein, M.; Ullrich, A.; Kaz, T.; Roduner, E. In-Situ Spin Trap Electron Paramagnetic Resonance Study of Fuel Cell Processes. *Phys. Chem. Chem. Phys.* **2004**, *6* (11), 2891.

(96) Zaton, M.; Rozière, J.; Jones, D. Current Understanding of Chemical Degradation Mechanisms of Perfluorosulfonic Acid Membranes and Their Mitigation Strategies: A Review. *Sustain. Energy Fuels* **2017**, 409–438.

(97) Zhang, K.; Yue, Q.; Chen, G.; Zhai, Y.; Wang, L.; Wang, H.; Zhao, J.; Liu, J.; Jia, J.; Li, H. Effects of Acid Treatment of Pt−Ni Alloy Nanoparticles@Graphene on the Kinetics of the Oxygen Reduction Reaction in Acidic and Alkaline Solutions. *J. Phys. Chem. C* **2011**, *115* (2), 379–389.

(98) Zhou, M.; Yu, Y.; Hu, K.; Mirkin, M. V. Nanoelectrochemical Approach To Detecting Short-Lived Intermediates of Electrocatalytic Oxygen Reduction. *J. Am. Chem. Soc.* **2015**, *137* (20), 6517–6523.

(99) Percival, S. J.; Dick, J. E.; Bard, A. J. Cathodically Dissolved Platinum Resulting from the O2 and H2O2 Reduction Reactions on Platinum Ultramicroelectrodes. *Anal. Chem.* **2017**, *89* (5), 3087–3092.

(100) Briega-Martos, V.; Herrero, E.; Feliu, J. M. Effect of pH and Water Structure on the Oxygen Reduction Reaction on Platinum Electrodes. *Electrochim. Acta* **2017**, *241*, 497–509.

(101) Zhao, Z.; Castanheira, L.; Dubau, L.; Berthomé, G.; Crisci, a.; Maillard, F. Carbon Corrosion and Platinum Nanoparticles Ripening under Open Circuit Potential Conditions.

J. Power Sources **2013**, *230*, 236–243.

(102) Alayan, R.; Arnaud, L.; Broyer, M.; Cottancin, E.; Lermé, J.; Marhaba, S.; Vialle, J.; Pellarin, M. Organization of Size-Selected Platinum and Indium Clusters Soft-Landed on Surfaces. *Phys. Rev. B* **2007**, *76* (7), 1–8.

(103) Tainoff, D.; Bardotti, L.; Tournus, F. Self-Organization of Size-Selected Bare Platinum Nanoclusters: Toward Ultra-Dense Catalytic Systems. *J. Phys. Chem. C* **2008**, *112*, 6842–6849.

(104) Bardotti, L.; Tournus, F.; Mélinon, P.; Pellarin, M.; Broyer, M. Mass-Selected Clusters Deposited on Graphite: Spontaneous Organization Controlled by Cluster Surface Reaction. *Phys. Rev. B* **2011**, *83* (3), 35425.

(105) Ding, W.; Dikin, D. a.; Chen, X.; Piner, R. D.; Ruoff, R. S.; Zussman, E.; Wang, X.; Li, X. Mechanics of Hydrogenated Amorphous Carbon Deposits from Electron-Beam-Induced Deposition of a Paraffin Precursor. *J. Appl. Phys.* **2005**, *98* (1), 14905.

(106) Griffiths, A. J. V; Walther, T. Quantification of Carbon Contamination under Electron Beam Irradiation in a Scanning Transmission Electron Microscope and Its Suppression by Plasma Cleaning. *J. Phys. Conf. Ser.* **2010**, *241* (Emag 2009), 12017.

(107) Lai, S. C. S.; Lazenby, R. A.; Kirkman, P. M.; Unwin, P. R. Nucleation, Aggregative Growth and Detachment of Metal Nanoparticles during Electrodeposition at Electrode Surfaces. *Chem. Sci.* **2015**, *6* (2), 1126–1138.

(108) Kim, Y. R.; Lai, S. C. S.; McKelvey, K.; Zhang, G.; Perry, D.; Miller, T. S.; Unwin, P. R. Nucleation and Aggregative Growth of Palladium Nanoparticles on Carbon Electrodes:

Experiment and Kinetic Model. *J. Phys. Chem. C* **2015**, *119* (30), 17389–17397.

(109) Zhao, Z.; Dubau, L.; Maillard, F. Evidences of the Migration of Pt Crystallites on High Surface Area Carbon Supports in the Presence of Reducing Molecules. *J. Power Sources* **2012**, *217*, 449–458.

(110) Giesen, M. Step and Island Dynamics at Solid/vacuum and Solid/liquid Interfaces. *Prog. Surf. Sci.* **2001**, *68* (1–3), 1–154.

(111) Kang, M.; Perry, D.; Kim, Y. R.; Colburn, A. W.; Lazenby, R. A.; Unwin, P. R. Time-Resolved Detection and Analysis of Single Nanoparticle Electrocatalytic Impacts. *J. Am. Chem. Soc.* **2015**, *137* (34), 10902–10905.

(112) Ustarroz, J.; Kang, M.; Bullions, E.; Unwin, P. R. Impact and Oxidation of Single Silver Nanoparticles at Electrode Surfaces: One Shot versus Multiple Events. *Chem. Sci.* **2017**, *8* (3), 1841–1853.

(113) Loget, G.; Kuhn, A. Electric Field-Induced Chemical Locomotion of Conducting Objects. *Nat. Commun.* **2011**, *2*, 535.

(114) Loget, G.; Zigah, D.; Bouffier, L.; Sojic, N.; Kuhn, A. Bipolar Electrochemistry: From Materials Science to Motion and beyond. *Acc. Chem. Res.* **2013**, *46* (11), 2513–2523.

(115) Loget, G.; Kuhn, A. Propulsion of Microobjects by Dynamic Bipolar Self-Regeneration. *J. Am. Chem. Soc.* **2010**, *132* (45), 15918–15919.

(116) Fattah, Z.; Loget, G.; Lapeyre, V.; Garrigue, P.; Warakulwit, C.; Limtrakul, J.; Bouffier, L.; Kuhn, a. Straightforward Single-Step Generation of Microswimmers by Bipolar Electrochemistry. *Electrochim. Acta* **2011**, *56* (28), 10562–10566.

(117) Paxton, W. F.; Sen, A.; Mallouk, T. E. Motility of Catalytic Nanoparticles through Self-Generated Forces. *Chem. - A Eur. J.* **2005**, *11* (22), 6462–6470.

(118) Wang, Y.; Hernandez, R. M.; Bartlett, D. J.; Bingham, J. M.; Kline, T. R.; Sen, A.; Mallouk, T. E. Bipolar Electrochemical Mechanism for the Propulsion of Catalytic Nanomotors in Hydrogen Peroxide Solutions. *Langmuir* **2006**, *22* (25), 10451–10456.

(119) Duan, W.; Wang, W.; Das, S.; Yadav, V.; Mallouk, T. E.; Sen, A. Synthetic Nano- and Micromachines in Analytical Chemistry: Sensing, Migration, Capture, Delivery, and Separation. *Annu. Rev. Anal. Chem.* **2015**, *8* (1), 311–333.

(120) Wang, W.; Duan, W.; Ahmed, S.; Sen, A.; Mallouk, T. E. From One to Many: Dynamic Assembly and Collective Behavior of Self-Propelled Colloidal Motors. *Acc. Chem. Res.* **2015**, *48* (7), 1938–1946.

(121) Paxton, W. F.; Kistler, K. C.; Olmeda, C. C.; Sen, A.; St. Angelo, S. K.; Cao, Y.; Mallouk, T. E.; Lammert, P. E.; Crespi, V. H. Catalytic Nanomotors: Autonomous Movement of Striped Nanorods. *J. Am. Chem. Soc.* **2004**, *126* (41), 13424–13431.

Insert Table of Contents Graphic and Synopsis Here